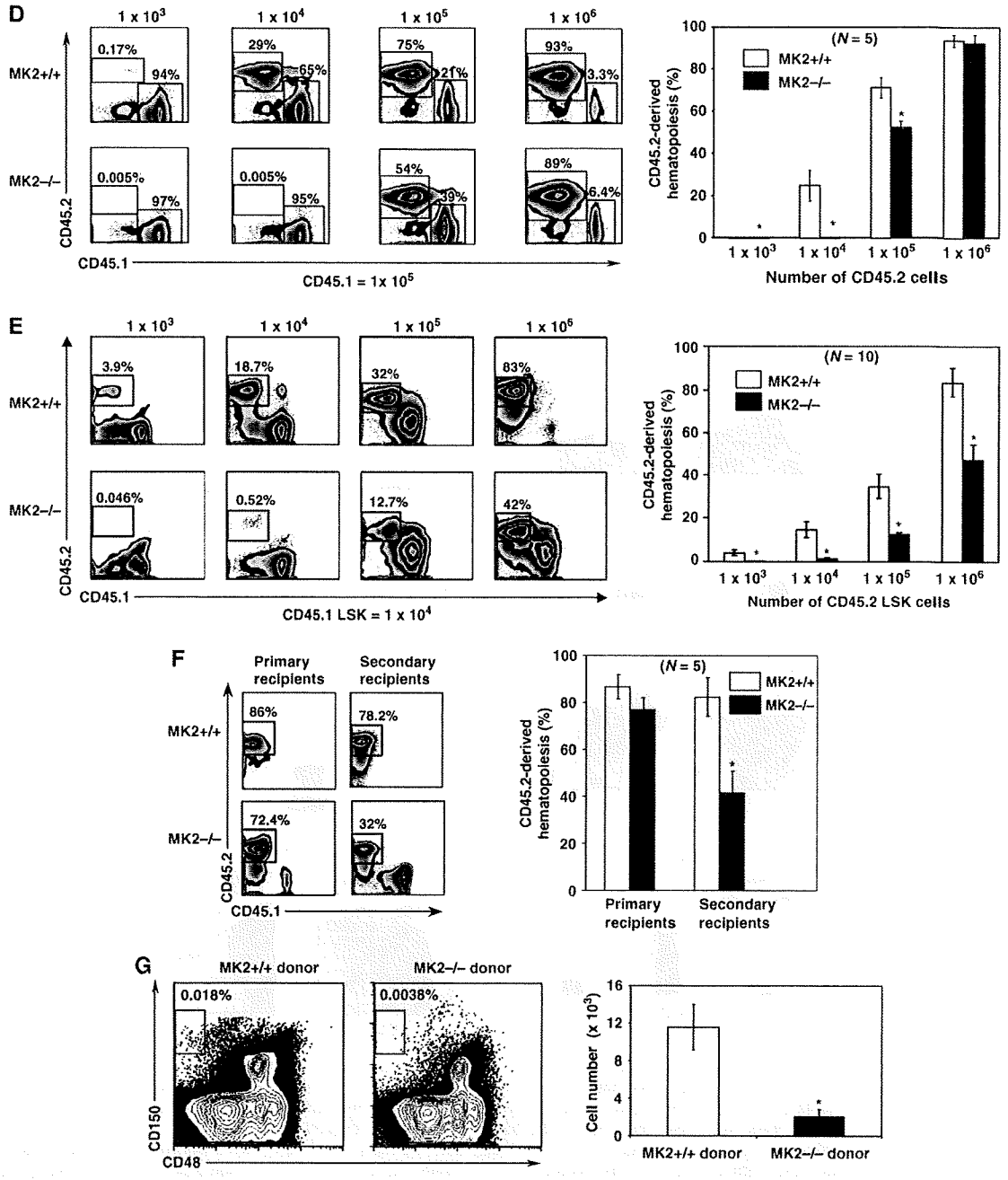

Figure 3 Continued.

difference between MK2-deficient cells and wildtype cells was striking (0.005 versus 29% for 10^4 HSCs and 0.005 versus 0.17% for 10^3 HSCs) (Figure 3D). Hence, MK2−/− HSCs showed an obvious disadvantage in their repopulation capacity, when compared with wild-type cells. To confirm and to further extend this finding, the repopulation experiment was also carried out with the LSK cell fraction enriched in HSCs. A similar defect was observed with respect to the LSK-repopulation capacity of MK2−/− cells (Figure 3E). We also carried out a secondary transplant experiment to confirm the self-renewal capacity of HSCs. Mice transplanted with a cell population of 2×10^6 WT and MK2−/− bone marrow cells (CD45.2) mixed with 10^5 competitor cells showed a mild reduction of CD45.2-positive MK2−/− cells compared with WT cells 12 weeks after transplantation (Figure 3F, primary recipients). When 2×10^6 bone marrow cells of these primary recipients were transplanted into secondary recipients, a defect of MK2−/− HSC became manifest (32% CD45.2 MK2−/− cells versus 78% CD45.2 MK2+/+ cells) (Figure 3F, secondary recipients), almost independently of addition of wild-type competitor cells (Supplementary Figure 9). Finally, the restoration of the CD150+CD48− HSC compartment after transplantation into WT mice, depending on the genotype of the donor cells, was analysed and was shown to be reduced for MK2-deficient donor cells (Figure 3G). Together these experiments show that a decreased quiescent

HSC pool in MK2−/− mice results in functional impairment under stress conditions.

Identification of Edr1 and Edr2 as interaction partners of MK2

To identify new interacting proteins for mouse MK2, a yeast-two-hybrid screen was carried out using a murine day-11-embryo brain library. The analysis revealed 27 positive clones: three of them carried cDNAs of the known MK2-interaction partner p38α, 17 clones carried 11 different cDNA fragments coding for C-terminal parts of mouse Edr1 ($n=4$), p36-Edr2 ($n=6$) and p90-Edr2 (Yamaki *et al*, 2002) ($n=1$). Interestingly, all Edr1/2 clones contained a single zinc-finger domain with the FCS signature followed by the region coding for the C-terminal homology domains (HD) II and III. HDII is also known as a sterile alpha motif (SAM) domain that has been shown to self-associate, bind to other SAM domains or form heteromeric interactions with some non-SAM domains of other proteins (Qiao and Bowie, 2005). The specificity of MK2–Edr1/2 interaction was confirmed by GST-pull-down experiments upon recombinant expression in *Escherichia coli*, using His–p38α/GST–MK2 interaction as a positive control. As shown in Figure 4A, His-Edr1 and His-Edr2 specifically bind to GST-MK2 but not to GST. In subsequent experiments, we limited our investigations to Edr2 interactions, as ectopic overexpression of Edr1 in mammalian cells was inefficient and available antibodies showed a low degree of specificity. Specific interaction of MK2 with endogenous Edr2 was shown by GST pull-down of endogenous Edr2 from HEK293-T cells transfected with different GST constructs (Figure 4B). Although endogenous Edr2 was found to bind to GST-MK2 and to the GST fusion of the structurally closely related MK3, which is expressed in LSK cells at levels comparable to MK2 (Supplementary Figure 10), as well as to the PcG member GST–Bmi1—used here as a positive control, GST fusion of the structurally more distant MK5, GST-MK5, was not able to bind Edr2 efficiently. We then extended the analysis of MK2–Edr2 interaction by carrying out co-immunoprecipitation of endogenous MK2 and Edr2 from mouse embryonic fibroblasts (Figure 4C). The specificity of the positive signal is shown by inefficient co-immunoprecipitation from lysates of MK2/3-deficient fibroblasts.

MK2 interacts with PRC1

Next, we were interested to know whether MK2 interacts with Edr2 within the physiological PRC1 complex. To this end, we tried to detect another core component of PRC1, the ring finger protein Ring1B, in the protein fraction bound to GST-MK2. As a negative control, we used again a GST-MK5 pull-down. As shown in Figure 4D, MK2, but not MK5, precipitates Ring1B, supporting the notion that MK2 is able to interact with the physiological PRC1 complex. To rule out the possibility that this interaction is because of the ectopic overexpression of the recombinant fusion proteins, we analysed the co-existence of the endogenous proteins in high molecular-weight fractions from lysates of mouse embryonic fibroblasts (MEFs). Lysates were separated by gel filtration and protein fractions were analysed by western blot using antibodies against Ring1B and MK2 (Figure 4E). In lysates from wildtype MEFs, co-separation of Ring1B and a small sub-population of MK2 can be detected in a fraction corresponding to a molecular mass of about 1MDa (asterisk). To show the specificity of the bands for MK2, we repeated this analysis with lysate from MK2-deficient MEFs. Although Ring1B can be detected in the corresponding fraction, the two corresponding bands for MK2 (boxed) are missing. This supports the notion that a sub-population of endogenous MK2 exists in the 1-MDa fraction, reflecting its interaction with endogenous PRC1. This interaction obviously does not include p38 MAPK, as it cannot be detected in the 1-MDa fraction (data not shown).

Edr2 and MK2 co-localize in polycomb bodies characteristic for PRC1

MK2 and p38α exist as a complex in the nucleus of resting cells. Upon activation of the p38 MAPK cascade, MK2 is phosphorylated, activated, and because of de-masking of a nuclear export signal, translocates to the cytoplasm (Ben-Levy *et al*, 1998; Engel *et al*, 1998; Neininger *et al*, 2001). In view of this finding, we hypothesized that a physiologically relevant nuclear PRC1–MK2 interaction may be released upon activation of the p38 MAPK cascade. First, we analysed the sub-cellular localization of MK2 and Edr2 in quiescent HEK293 cells upon transfection with MK2–YFP and Edr2–CFP fusion constructs. Both proteins showed perfect co-localization in speckles in the nucleus (polycomb bodies), reminiscent of the characteristic distribution pattern of proteins organized in PRC1 complexes such as endogenous Edr1, Edr2, Bmi1 and Ring1B (Suzuki *et al*, 2002) (Figure 5A). Second, we visualized stress-dependent translocation of GFP-MK2 in HeLa cells co-transfected with HA-Edr2. In contrast to our hypothesis, arsenite-induced stress activation of the p38 MAPK cascade did not trigger complete translocation of MK2 into the cytoplasm. In strict dependence on Edr2 co-expression, a sub-fraction of MK2 was retained in the polycomb bodies (Figure 5B), suggesting that activated MK2 alone or in complex with p38 may also have a physiological function at the nuclear PRC1 (cf. also schematic presentation of Figure 7).

Identification of the Edr2-interacting region in MK2

To further dissect the molecular interaction between MK2 and Edr2, we carried out GST–Edr2 pull-down assays using GFP fusion proteins with defined MK2 subdomains. Two regions of the small lobe of the kinase, subdomains I–III (amino acids 29–99) and IV-V (amino acids 97–131), are sufficient to interact with Edr2 (Figure 6A and B), indicating that both regions contribute to the interaction. The specific role of these subdomains for interacting with Edr2 was further substantiated using a MK2/MK5 hybrid molecule. When amino acids 38–128 are replaced by the homologous region of MK5, the hybrid molecule no longer binds to Edr2, as shown in pull-down experiments (Figure 6C), as well as in the co-localization assay (Figure 6D). As these domains do not overlap with the C-terminal docking site for p38α at amino acids 371–375 (Tanoue *et al*, 2000), it is possible that MK2, Edr2 and p38 can form a ternary complex at PRC1.

Functional rescue of MK2-deficient HSCs requires Edr2-binding of MK2

Finally, we were interested to determine a direct functional link between the HSC phenotype of MK2−/− mice and the Edr2-binding properties of MK2. To address this issue, we made use of the MK2/5 hybrid molecule, which is unable to

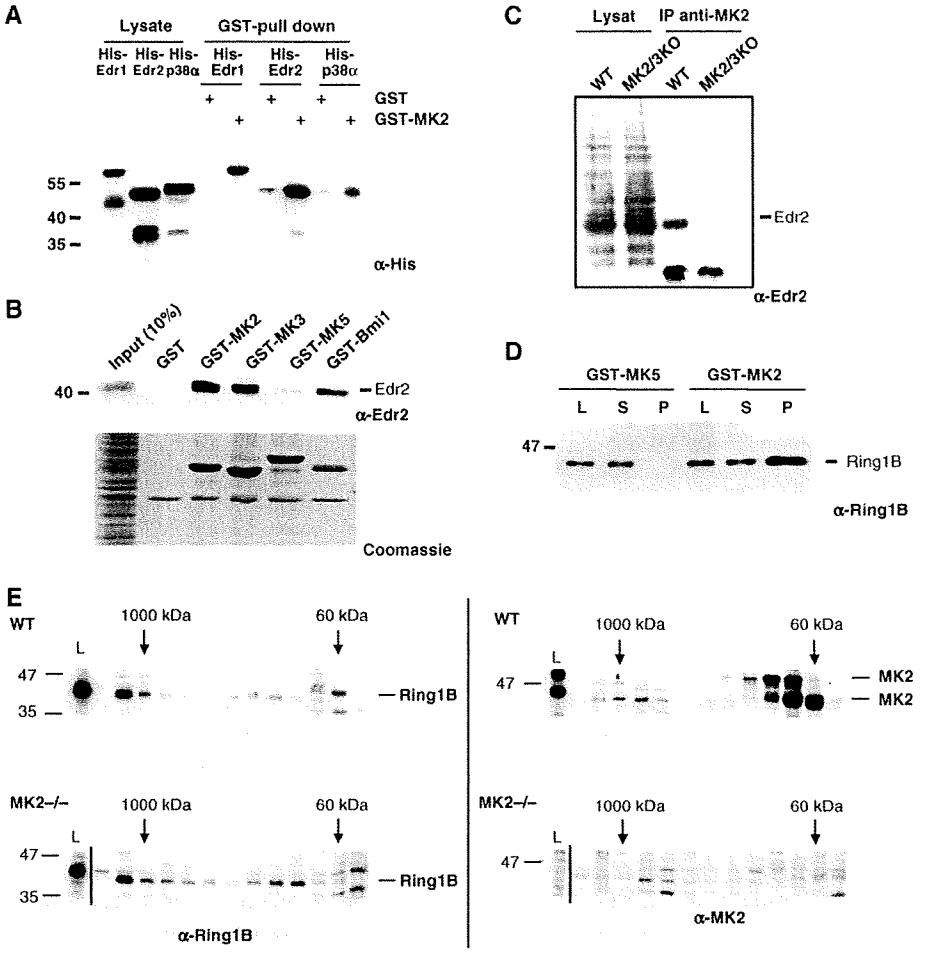

Figure 4 Interaction of MK2 with PRC1 components. (**A**) MK2 interaction with recombinant Edr1 and Edr2 *in vitro*. GST pull-down (right) of recombinant 6-His-tagged Edr1/2 from *E. coli* lysate. As a positive control, 6-His-tagged p38α is used; as negative control pull-down is performed with GST alone. Total *E. coli* lysates are separated at the left. His-tagged proteins are detected by anti-hexahistidine western blot. (**B**) Interaction of MK2 with endogenous Edr2. Whole-cell lysate of transfected HEK 293-T cells were used in a GST pull-down with recombinant GST-MK2, GST-MK3, GST-MK5, GST (negative control) and GST-Bmi1 (positive control). Comparable expression and GST pull down of the fusion proteins was monitored by Coomassie protein staining. Specific interactions of GST-MK2, GST-MK3 and GST-Bmi1 with endogenous Edr2 were detected by western blot using Edr2 antibodies. (**C**) Co-IP of endogenous MK2 and Edr2 from WT mouse embryonic fibroblasts (MEFs) but not from MK2/3-deficient (MK2/3 KO) MEFs (negative control). (**D, E**) MK2 interaction with the PRC1 complex. (D) Lysates (L) from HEK 293 cells overexpressing Edr2 were subjected to GST pull-down using GST-MK2 and, as negative control, GST-MK5. Supernatant (S) and pull-down (P) were analysed for PRC1 complexes by western blot against the PRC1 component Ring1B. (E) Co-separation of endogenous Ring1B and endogenous MK2 in a high-molecular-weight fraction. Nuclear extracts from wildtype (WT) and MK2-deficient MEFs (MK2−/−) were applied to FPLC gel filtration using a Superose 6 HR 10/30 column. Proteins from load (L) and fractions were subsequently separated by SDS–PAGE. In both lower panels, an empty lane between load and fractions was cut out from the blot to align corresponding molecular-weight fractions between the analysis of WT (upper panel) and MK2-deficient (lower panel) cells. Ring1B and MK2 were detected by western blot. The approximate size of the native proteins in the chromatographic fractions is indicated on the top. The protein size in SDS–PAGE is indicated left. The Ring1B band and the two MK2-specific bands are indicated at the right of each blot. The bands representing the sub-population of MK2 in the high-molecular-weight fraction are marked by a box with asterisk in the anti-MK2 blot of separation of WT lysate. The corresponding region of separation of MK2-deficient lysate lacking these bands is also boxed. The MK2 antibody decorates also several bands in the lysate of MK2-deficient cells (MK2−/−) probably because of cross-reaction with MK3 and because of non-specific binding.

associate with Edr2 (see Figure 6C and D) but maintains full catalytic kinase activity, as shown in MK2/3 double knockout cells (Figure 6E). MK2/3 double-knockout embryonic fibroblasts do not display any stress-induced Hsp25 phosphorylation. In contrast, retrovirus-mediated expression of MK2/5 and MK2 yielded a comparable level of Hsp25 phosphorylation upon UV stimulation. Hence, MK2 and MK2/5 are indistinguishable with respect to their kinase activity and differ only in Edr2 binding, allowing the dissection of kinase function from Edr2-mediated effects in the MK2/5 hybrid kinase. We hypothesized that MK2-deficient cells would be reconstituted by MK2 but not by the MK2/5 hybrid kinase with respect to stem-cell fitness.

The viral constructs were then used to introduce MK2 and MK2/5 into lineage-marker negative MK2-deficient CD45.2 cells, yielding similar transduction rates (30%) as assessed by expression of the marker gene GFP. 10^4 bi-cistronic expression construct-transduced CD45.2 MK2-deficient LSK cells were mixed with the same number of control GFP-construct-transduced CD45.1 LSK WT competitor cells, transplanted into lethally irradiated CD45.1 recipient mice, which were analysed 3 month later. As seen in Figure 6F,

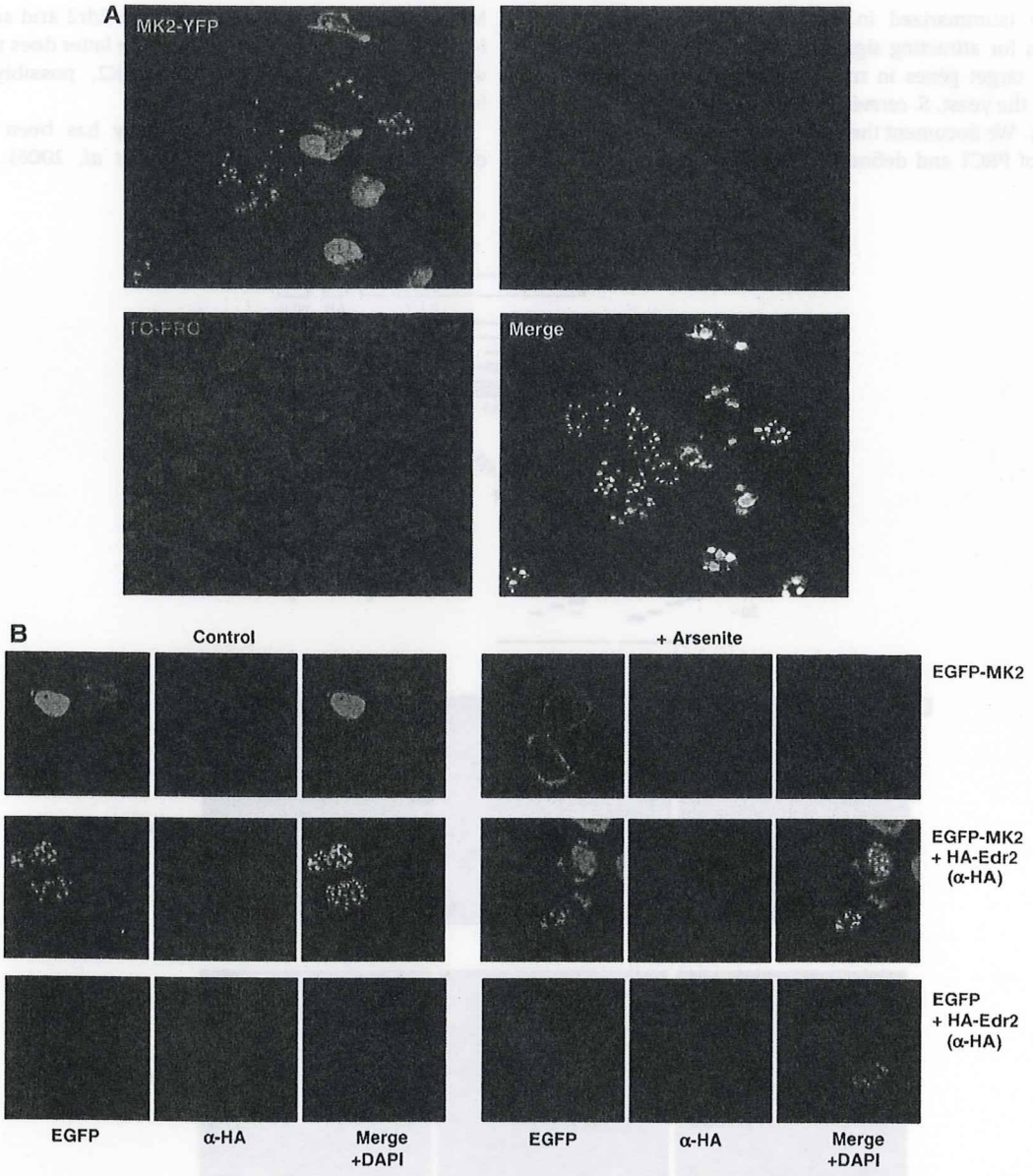

Figure 5 Co-localisation of MK2 and Edr2 in polycomb bodies characteristic for PRC1. (**A**) HEK 293 cells were transfected with constructs coding for an MK2-yellow fluorescent protein (YFP) fusion and an Edr2-CyAn fluorescent protein (CFP) fusion. Fusion proteins were visualized by fluorescence microscopy. Nuclei were stained using TO-PRO. (**B**) Stress-dependent changes in subcellular localizations of a GFP–MK2 fusion protein (GFP-MK2) in HeLa cells in the absence and presence of HA-tagged Edr2 (HA-Edr2). In the absence of HA-Edr2, arsenite treatment (+Arsenite) leads to export of evenly distributed GFP-MK2 from the nucleus. In cells overexpressing HA-Edr2 (+HA-Edr2), GFP–MK2 accumulates in polycomb bodies already before stress treatment (−Ars). Upon stress and in the presence of HA-Edr2, MK2 is translocated to the cytoplasm, but a sub-population of MK2 remains in polycomb bodies.

the LSK repopulation capacity of MK2−/− cells (6.8% in experiment 1 ($N=3$); 4.1% in experiment 2 ($N=3$)) is significantly increased by re-introduction of MK2 (42 and 49%), but not by the re-introduction of the Edr2 non-binding mutant of MK2, MK2/5 (0.4 and 0.2%). Taken together, this indicates that MK2–Edr2 interaction is essential for LSK repopulation capacity.

Discussion

MK2 is a downstream component of the p38 MAPK signalling cascade with pleiotropic functions. Acting as a protein kinase, MK2 controls the regulation of the actin cytoskeleton (Stokoe *et al*, 1992; Guay *et al*, 1997), stress-dependent small heat-shock protein phosphorylation (Vertii *et al*, 2006), and stability and translation of the AU-rich element containing cytokine mRNAs (Neininger *et al*, 2002; Hitti *et al*, 2006). Independently of its catalytic activity, MK2 stabilizes p38α (Kotlyarov *et al*, 2002) and could act as a shuttling protein, mediating nuclear export of p38α (Ben-Levy *et al*, 1998).

Here, we propose a new function for MK2 in maintaining HSC quiescence. This function involves MK2-targeting to PRC-1 through Edr1/2 binding and subsequent modulation of the transcriptional control mechanisms governing HSC

quiescence (summarized in Figure 7). This represents a mechanism for attracting signal-transducing protein kinases to specific target genes in mammalian cells as already described for the yeast, *S. cerevisiae* (Pokholok *et al*, 2006; Proft *et al*, 2006). We document the specific interaction of MK2 and members of PRC1 and define the regions involved in Edr2–MK2 interaction as a SAM domain on Edr2 and subdomains I–V in the small lobe of the kinase. The latter does not overlap with the p38α docking site on MK2, possibly allowing formation of a ternary complex.

Recently, the p38 MAPK pathway has been shown to control the lifespan of HSCs (Ito *et al*, 2006). Sustained

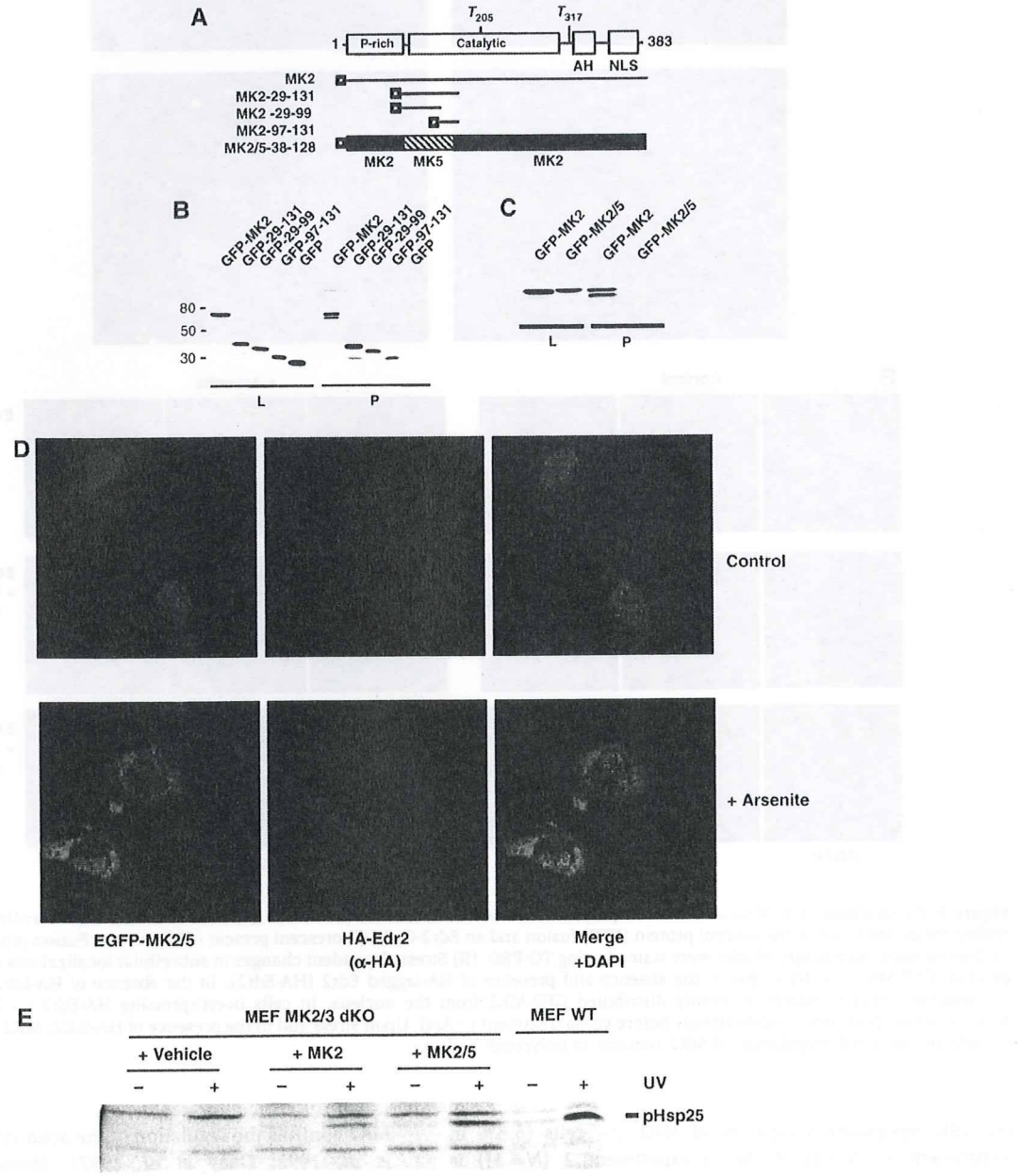

Figure 6 Identification of the Edr2-interacting region in MK2 and rescue of the repopulation capacity of MK2-deficient cells by MK2, but not by MK2/5. (**A**) Schematic representation of GFP–MK2, different GFP-tagged fragments of MK2, as well as an MK2/MK5 hybrid kinase (*P*-rich is the proline-rich N-terminal region, AH is the auto-inhibitory C-terminal helix containing the nuclear export signal (NES; Engel *et al*, 1998), NLS represents the nuclear localization signal and T205 and T317 are the regulatory phosphorylation sites of mouse MK2). (**B**, **C**) Lysates (*L*) from HEK 293 cells expressing the different GFP-tagged constructs described in (A) were subjected to GST-Edr2 pull-down (P). Proteins were detected by anti-GFP western blot. Molecular masses (kDa) are indicated in the left. (**D**) Comparable enzymatic activity of MK2 and MK2/5 against the *in vivo* substrate Hsp25 detected in transduced MEFs after UV stimulation (200 J/m^2) and 30 min recovery. (**E**) MK2/5 hybrid kinase misplaced from polycomb bodies (examined as in Figure 5B). (**F**) Competitive repopulation assay. 1×10^4 CD45.1 + LSK cells transduced with pMMP–IRES–GFP together with 1×10^4 CD45.2 + LSK cells transduced with the different bicistronic constructs indicated at the left were transplanted into recipient mice (CD45.1 +) and analysed for repopulation capacity as described. Two characteristic experiments and statistical evaluation (right) ($N = 6$) are shown. Asterisks indicate significant differences ($P < 0.01$) to vehicle-transduced cells. Transfection efficiency (about 30% for all three constructs) was monitored by GFP-expression.

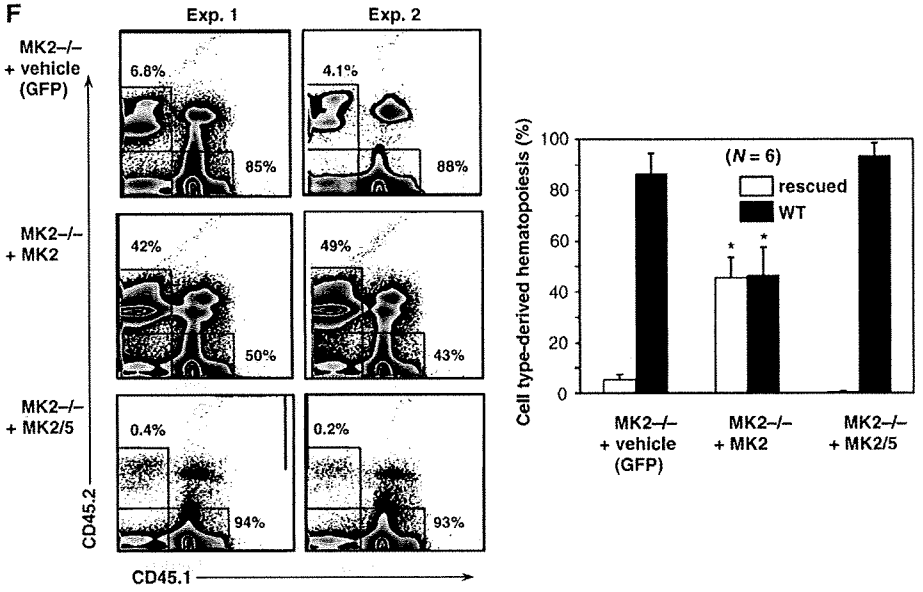

Figure 6 Continued.

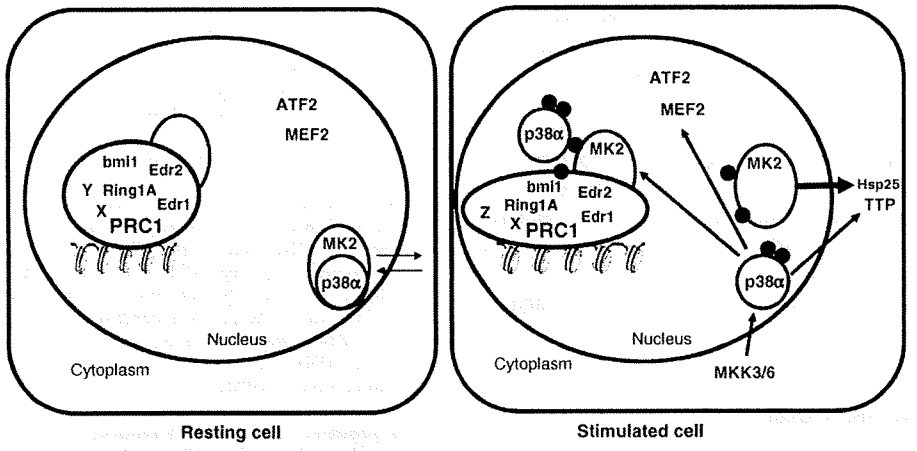

Figure 7 The model of stress -signalling to PRC1: In the nucleus of resting cells, a sub-population of MK2 (and MK3) is associated to PRC1 via specific interaction to Edr2 (and/or Edr1). A distinct, probably more abundant sub-population of MK2 (and MK3) exists in complex with p38α (or p38β). On stimulation of the p38 pathway, p38 is phosphorylated by MKK3 or MKK6 and, in turn, phosphorylates MK2 (and MK3). As a result of phosphorylation, the p38/MK2 complex becomes unstable (Lukas *et al*, 2004), the nuclear export signal of MK2 is unmasked (Neininger *et al*, 2001; White *et al*, 2007) and the sub-population of MK2 formerly bound to p38 is exported to the cytoplasm meeting its substrates such as Hsp25 and mRNA-binding proteins as tristetraprolin (TTP) (Hitti *et al*, 2006). Activated p38 may partially leave the nucleus (Ben-Levy *et al*, 1998), but also remains in the nucleus to phosphorylate transcription factors, such as ATF2 (Raingeaud *et al*, 1996) or MEF2 (Zhao *et al*, 1999), as well as PRC1-bound MK2/3. Activation of PRC-bound MK2/3 by p38 leads to phosphorylation of components of PRC1, such as Bmi1 (Voncken *et al*, 2005), and contributes to chromatin remodelling. Black balls symbolize phosphorylations.

activation of p38 MAPK under oxidative stress, which is probably paralleled by increased cytoplasmic accumulation of p38/MK2 complexes (Ben-Levy *et al*, 1998) and, hence, by their reduction at the PRC1, induces loss of 'stemness', similar to our findings in MK2-deficient mice. Thus, our analysis of MK2-deficient HSC may provide a missing link between the stress-induced MAPK pathway and Bmi1-controlled HSC maintenance.

It has been shown that the protein kinase MK3/3pK, which is closely related to MK2 and shows 75% identity in primary structure, is able to directly phosphorylate His-tagged Bmi1 *in vitro* at as yet unidentified sites (Voncken *et al*, 2005). In light of this observation, the MK2 could directly phosphorylate Bmi1 *in vivo*, as both enzymes share activators and substrates (Clifton *et al*, 1996; Ronkina *et al*, 2007).

Physiologically, we identified a new role for MK2 in maintaining HSC quiescence. Although we could show that the haematopoietic differentiation program seems to be intact in MK2-deficient cells, we identified a selective deficiency of the HSC compartment, as shown by decreased numbers of HSCs in MK2-deficient mice. Furthermore, we defined an increased fraction of proliferating cells in the early haematopoietic progenitor cell pool as well as increased *in vitro* proliferation, suggesting that MK2 is needed to put brakes on a state of quiescence by modulating the PRC1 complex. As a consequence of MK2 deficiency, 'stemness' is lost, as the

HSC's long-term engraftment and repopulation potential resides predominantly in the G0 fraction (Passegue, 2005). Mechanistically, we propose that targeting of the MK2 to PRC1 is responsible for the observed effects on HSCs. This idea is supported by our finding that the Edr2-binding domain of MK2 is necessary to rescue the repopulation capacity of MK2−/− LSK cells. Interestingly, it seems that the Edr2-non-binding mutant MK2/5 even suppresses repopulation capacity. We speculate that this could be because of the interference with MK3 action, which might, to a certain degree, functionally compensate for the loss of MK2. This idea is supported by the comparable expression of MK2- and MK3-mRNA in LSK cells (Supplementary Figure 10) and comparable Edr2-binding (Figure 4B) of both enzymes. However, a detailed analysis of the effects of the MK2/5 mutant in WT cells will be necessary to further substantiate this speculation.

Few extrinsic and intrinsic factors have been implicated in controlling HSC maintenance (Suda *et al*, 2005; Adams and Scadden, 2006). Bmi1, a component of PRC1, is a crucial molecule in governing 'stemness' of HSC (van der Lugt *et al*, 1994; Lessard and Sauvageau, 2003; Iwama *et al*, 2004) and neuronal stem cells (Molofsky *et al*, 2003). Interestingly, in contrast to Bmi1-deficient stem cells, the Ink4a locus as a downstream target of Bmi1 (Jacobs *et al*, 1999; Park *et al*, 2003), encoding p16Ink4a and p19Arf under the control of two distinct promoters (Quelle *et al*, 1995), is selectively affected in MK2-deficient HSC: Only the expression of p19Arf, a protein involved in p53-dependent apoptosis, is increased. The reason for this selectivity is currently unknown, but it might reflect the difference between Bmi1 deletion and loss of Bmi1 phosphorylation, or a different as-yet unknown function of MK2. Regardless of the molecular mechanism, MK2 emerges as a new important player and potential target to be manipulated in normal and malignant haematopoiesis.

Materials and methods

Mice

Mapkapk2^{tm1Mgl} mice (C57/Bl6) representing the conventional complete knockout of MK2 (Kotlyarov *et al*, 1999) were bred and maintained under specific pathogen-free conditions in the central animal facility at Hannover Medical School. In all experiments, age- and sex-matched mice were used at 4–12 weeks of age. All experiments were approved by the institutional review board.

Cell sorting and culture

For *in vitro* studies, purified SLAM (CD150+CD48−) or Lin$^-$Sca1$^+$c-kit$^+$ cells from MK2+/+ and MK2−/− mice were cultured in IMDM medium supplemented with 10% FCS, 2 mM L-glutamine, 1% penicillin–streptomycin, 1 mM non-essential amino acids, 10 ng/ml rm-IL3, 10 ng/ml rm-IL6, 50 ng/ml rm-SCF, 50 ng/ml and rh-Flt3L (all from Peprotech, Rocky Hill, NJ).

For *in vitro* proliferation experiments, LSK cells were cultured for 48 h as mentioned above and subsequently pulsed with 1 μCi ^{3}H-thymidine for 12 h. Incorporated ^{3}H-thymidine was quantified by scintillation counting.

For p38 inhibitor studies, Lin$^-$Sca1$^+$c-kit$^+$ cells from MK2+/+ mice were sorted and cultured either in the presence or in the absence of SB239063 (5 μM, Calbiochem) for 72 h.

For cell-cycle analysis, sorted LSK cells were cultured for 48 h *in vitro* and fixed with ice-cold absolute ethanol for 1 h on ice. Cells were washed, incubated with propidium iodide (0.5 μg/ml, Sigma) and RNase A (5 μg/ml, Qiagen) for 1 h, and analysed by flow cytometry.

Side population (SP) studies

SP studies were conducted as described earlier (Goodell *et al*, 1996). Briefly, RBC-depleted total bone marrow cells of MK2+/+ and MK2−/− mice were re-suspended in pre-warmed DMEM medium containing Hoechst 33342 dye (5 μg/ml, Sigma) either in the presence or in the absence of verapamil (50 μM, Sigma) and incubated for 90 min at 37°C. Cells were washed twice with ice-cold HBSS, stained with propidium iodide (2 μg/ml) and analysed by a Moflo cell sorter (DAKO Cytomation, Glostrup, Denmark).

Flow cytometry

Single cell suspensions were analysed by flow cytometry using FACS SCAN or FACS Canto and CELLQuest software, FACS Diva software (BD Biosciences) or FlowJo software (Tree Star, Inc., Ashland, OR). Cell sorting of defined sub-populations was carried out using the Moflo cell sorter with Summit software or FACSAria cell sorter (BD Biosciences). The following monoclonal antibodies (all from BD Pharmingen, San Diego, CA except noted otherwise) were used: CD3ε-biotin, CD-4-biotin, CD8-biotin, CD11b-biotin, CD11c-biotin, CD19-biotin, CD48-biotin (eBiosciences, San Diego, CA), CD117-APC, CD150-PE (eBiosciences), B220-biotin, Gr-1-biotin, Sca-1-PE and TER119-biotin.

BrdU incorporation

In vivo incorporation of BrdU into LSK cells was assessed using the FITC BrdU Flow kit (BD Pharmingen). After a single intraperitoneal injection of BrdU (Sigma, 1 mg per 6 g of mouse weight), an admixture of 1 mg/ml of BrdU was added to the drinking water for 3 days. Mice were killed, BM cells were prepared and stained with antibodies recognizing lineage, Scal and c-kit markers, and analysed by flow cytometry.

CFSE proliferation assay

For CFSE studies, purified CD150+CD48− cells were labeled with 2 mM CFSE (Molecular Probes, Karlsruhe, Germany) in IMDM complete medium at 37°C for 10 min. Cells were washed with PBS, cultured as indicated above and analysed by flow cytometry.

RNA isolation and real-time PCR

Total RNA was isolated using commercially available kit systems (Absolutely RNA mini prep kit,Stratagene, La Jolla, CA). cDNA was synthesized using oligo-dT primer and expand reverse transcriptase (Roche). p19 and p21 expression levels were determined by real-time PCR using the primers described in Supplementary data. The PCR reaction was carried out in duplicates using a LightCycler-FastStart DNA Master SYBR Green I kit (Roche) according to the manufacturer's instructions.

Competitive repopulation studies

Defined numbers of (i) RBC-depleted donor (CD45.2) BM or of (ii) LSK cells of 8-week-old MK2+/+ and MK2−/− mice or (iii) 10^4 MK2−/− LSK cells transduced with the bicistronic pMMP-IRES viral construct (see below) were mixed with (i) 10^5 competitor bone marrow or (ii) 10^4 competitor LSK cells or (iii) 10^4 LSK cells transduced with the viral GFP-expressing control construct (CD45.1) cells, respectively, and transplanted i.v. into lethally irradiated (10 Gy) congenic recipients (CD45.1). In the LSK repopulation experiments ((ii) and (iii)), 10^5 total-BM-compensatory carrier cells (CD45.1) were added to the cell mixture to create a supportive environment during the initial period after transplantation and to increase the viability of the transplanted animals. The number of stem cells in these compensatory cells is negligibly small compared with the number of stem cells in the LSK populations. Transplanted mice were maintained under specific pathogen-free conditions for 3 months. For secondary transplantation, 2×10^6 BM cells were transplanted into lethally irradiated congenic recipients and 12 weeks after transplantation, 2×10^6 BM cells were isolated, analysed for CD45.2 derived cells and subsequently transplanted into lethally irradiated congenic secondary recipients. At 16 weeks after transplantation, BM of secondary recipients was analysed for CD45.2-derived cells.

Yeast two-hybrid screen

A mouse-brain library (MY4008AH, MATCHMAKER, Clontech) in strain Y187 (MATα) was mated with pGBKT7-MK2 to identify the interaction partners of mouse MK2. About 2.5×10^7 colonies that contained 3.5×10^6 independent cDNA clones were screened.

Transfections, pull-down and co-immunoprecipitation

HEK293-T and HeLa cells were cultured and transfected as described (Schumacher *et al*, 2004). For *in vitro* pull-down assays, a total of 1×10^7 transfected HEK293-T cells expressing GST-tagged MK2, MK3, MK5 or Bmi1 were used and GST pull-down was carried out as described (Schumacher *et al*, 2004). Bound proteins were analysed by western blot using antibodies against Edr2 or Ring1B (Atsuta *et al*, 2001). Alternatively, purified recombinant hexahistidine-tagged Edr1, Edr2 or p38 proteins were incubated with recombinant GST or GST-tagged MK2 protein bound to glutathione Sepharose 4B beads. Binding of His-fusion proteins was detected by western blot using 6x-His antibodies (Clontech). For co-IP, 2×10^7 immortalized WT or MK2/3 double-knockout MEFs were lysed in 1.3 ml buffer (50 mM HEPES (pH 7.5), 1% Triton X-100, 10% glycerol, 150 mM NaCl, 1.5 mM $MgCl_2$, 1 mM EGTA). In all 2.5 mg of cell lysate was incubated with 5 µl of MK2 antibody (Cell Signaling3042) overnight at 4°C and subsequently incubated with 25 µl of protein G Sepharose (Amersham) for 1.5 h at 4°C. Beads were washed five times with cold lysis buffer and western blot was carried out using Edr2 antibody (Atsuta *et al*, 2001).

Gel filtration

In total, 4×10^7 immortalized WT or MK2−/− mouse embryonic fibroblasts (Kotlyarov *et al*, 1999) were lysed in 400 µl lysis buffer (20 mM HEPES pH 7.5, 50 mM KCl, 2 mM $MgCl_2$, 0.5% Nonidet P40, 0.5 mM DTT, protease inhibitor cocktail tablet (Roche Diagnostics)) and centrifued at 800 *g* for 8 min at 4°C. Supernatant was removed and the pelleted nuclei were lysed in Buffer A (50 mM HEPES pH 7.6, 250 mM NaCl, 10% glycerol, 0.5% Triton X-100, 1 mM EDTA, 1 mM DTT, protease inhibitor cocktail tablet (Roche Diagnostics)) for 20 min on ice. Nuclei were passed 10 times through a 20-gauge needle and centrifuged at 16 000 *g*, 4°C. In total, 500 µg of nuclear extract was separated by FPLC (LCC-500 Plus) using two Superose 6HR 30/10 columns connected in series (Pharmacia LKB Biotechnology, Uppsala, Sweden), developed with 0.05 M K_2HPO_4/KH_2PO_4, pH 7.2, 0.15M NaCl with a flow-rate of 0.1 ml/min. Proteins from fractions were precipitated by adding 1/100 volume of 2% deoxycholate, incubation for 30 min at 4°C and addition of 1/10 volume of 100% trichloroacetic acid. Samples were incubated overnight at 4°C, centrifuged for 15 min at 16 000 *g*, air-dried, dissolved in 4 × SDS sample buffer and separated by 10% SDS–PAGE. Western blotting was carried out using anti-Ring1B (Atsuta *et al*, 2001) and anti-MK2 (Cell Signaling 3042) antibodies.

Fluorescence microscopy

For subcellular localization of YFP- and CFP-tagged proteins, the transfected cells (with lipofectamine/plus reagent, Invitrogen) were replated in chambered coverglass (Lab-Tek, Nunc) and analysed using a Leica DM IRBE microscope with the Leica TCS confocal systems program. For immunocytochemistry, HeLa cells were seeded on poly-L-lysine-coated coverslips. At 24 h after transfection of EGFP- and HA-tagged proteins, cells were fixed with 4% paraformaldehyde and incubated overnight with HA antibodies (Santa Cruz, sc-805) followed by Alexa 555 (Invitrogen, A31572) staining.

Cloning, construction of deletion mutants and site-directed mutagenesis

Cloning techniques are described in detail in Supplementary data. For generation of deletion mutants, the fusion of amino acids 29–131, 29–99 and 97–131 of MK2 to EGFP was carried out by inserting *Eco*RI–*Bam*HI-cut PCR fragments, amplified from pEGFP-MK2 (Engel *et al*, 1995) using the primers given in Supplementary data, into pEGFP-C1 (Clontech). The pEGFP-MK2/MK5 hybrid was generated by deletion of MK2-amino acids 37–131 from pEGFP-MK2 using *Pst*I/*Sac*I and cloning of *Pst*I–*Sac*I-cut PCR fragment of MK5-amino acid 10–110, amplified with the primers given in Supplementary data.

Viral transductions of MEFs and L-negative cells

MEFs were tranduced with the retroviral constructs pMMP–IRES–GFP, pMMP–MK2–IRES–GFP and pMMP–MK2/5–IRES–GFP as described (Ronkina *et al*, 2007). pHsp25 was detected by western blotting using an anti-phosphoS86-Hsp25 antibody (BioSource). Before retroviral transduction, L-negative cells were stimulated with mSCF (100 ng/ml), hIL-11 (100 ng/ml) and hFlt3-Lig (100 ng/ml) for 48 h in StemSpan. Lin(−) Ly 5.1 cells were transduced with pMMP–IRES–GFP (MOI = 3) whereas Lin(−) Ly 5.2 were transduced with the different retroviral transfer vectors with MOI = 3 after 48 and 60 h. The Lin(−) transduced cells were sorted for Sca-1$^+$c-Kit$^+$LSK before mixing for repopulation assay.

Supplementary data

Further experimental data, data about plasmids and primers used for cloning and PCR as well as cloning details are provided in the Supplementary data. Supplementary Figures are provided. Supplementary data are available at *The EMBO Journal* Online (http://www.embojournal.org).

Acknowledgements

We thank David Luckhaus and Cosima Hakim for help with the initial two-hybrid screen and with the gel filtration experiments, respectively. Dr Matthias Ballmaier and the central cell-sorting facility at MHH are greatly acknowledged. This work was supported by grants from DFG SFB 566 and DFG KliFo 110.

References

Adams GB, Scadden DT (2006) The hematopoietic stem cell in its place. *Nat Immunol* **7:** 333–337

Atsuta T, Fujimura S, Moriya H, Vidal M, Akasaka T, Koseki H (2001) Production of monoclonal antibodies against mammalian Ring1B proteins. *Hybridoma* **20:** 43–46

Ben-Levy R, Hooper S, Wilson R, Paterson HF, Marshall CJ (1998) Nuclear export of the stress-activated protein kinase p38 mediated by its substrate MAPKAP kinase-2. *Curr Biol* **8:** 1049–1057

Blank U, Karlsson G, Moody JL, Utsugisawa T, Magnusson M, Singbrant S, Larsson J, Karlsson S (2006) Smad7 promotes self-renewal of hematopoietic stem cells. *Blood* **108:** 4246–4254

Boyer LA, Plath K, Zeitlinger J, Brambrink T, Medeiros LA, Lee TI, Levine SS, Wernig M, Tajonar A, Ray MK, Bell GW, Otte AP, Vidal M, Gifford DK, Young RA, Jaenisch R (2006) Polycomb complexes repress developmental regulators in murine embryonic stem cells. *Nature* **441:** 349–353

Cheng T, Rodrigues N, Shen H, Yang Y, Dombkowski D, Sykes M, Scadden DT (2000) Hematopoietic stem cell quiescence maintained by p21cip1/waf1. *Science* **287:** 1804–1808

Clifton AD, Young PR, Cohen P (1996) A comparison of the substrate specificity of MAPKAP kinase-2 and MAPKAP kinase-3 and their activation by cytokines and cellular stress. *FEBS Lett* **392:** 209–214

Duncan AW, Rattis FM, DiMascio LN, Congdon KL, Pazianos G, Zhao C, Yoon K, Cook JM, Willert K, Gaiano N, Reya T (2005) Integration of Notch and Wnt signaling in hematopoietic stem cell maintenance. *Nat Immunol* **6:** 314–322

Engel K, Kotlyarov A, Gaestel M (1998) Leptomycin B-sensitive nuclear export of MAPKAP kinase 2 is regulated by phosphorylation. *EMBO J* **17:** 3363–3371

Engel K, Schultz H, Martin F, Kotlyarov A, Plath K, Hahn M, Heinemann U, Gaestel M (1995) Constitutive activation of mitogen-activated protein kinase-activated protein kinase 2 by mutation of phosphorylation sites and an A-helix motif. *J Biol Chem* **270:** 27213–27221

Gaestel M (2006) MAPKAP kinases—MKs—two's company, three's a crowd. *Nat Rev Mol Cell Biol* **7:** 120–130

Goodell MA, Brose K, Paradis G, Conner AS, Mulligan RC (1996) Isolation and functional properties of murine hematopoietic stem cells that are replicating *in vivo*. *J Exp Med* **183:** 1797–1806

Guay J, Lambert H, Gingras-Breton G, Lavoie JN, Huot J, Landry J (1997) Regulation of actin filament dynamics by p38 map kinase-mediated phosphorylation of heat shock protein 27. *J Cell Sci* **110:** 357–368

Hegen M, Gaestel M, Nickerson-Nutter CL, Lin LL, Telliez JB (2006) MAPKAP kinase 2-deficient mice are resistant to collagen-induced arthritis. *J Immunol* **177:** 1913–1917

Hitti E, Iakovleva T, Brook M, Deppenmeier S, Gruber AD, Radzioch D, Clark AR, Blackshear PJ, Kotlyarov A, Gaestel M (2006) Mitogen-activated protein kinase-activated protein kinase 2 regulates tumor necrosis factor mRNA stability and translation mainly by altering tristetraprolin expression, stability, and binding to adenine/uridine-rich element. *Mol Cell Biol* **26:** 2399–2407

Hock H, Hamblen MJ, Rooke HM, Schindler JW, Saleque S, Fujiwara Y, Orkin SH (2004) Gfi-1 restricts proliferation and preserves functional integrity of haematopoietic stem cells. *Nature* **431:** 1002–1007

Isono K, Fujimura Y, Shinga J, Yamaki M, O-Wang J, Takihara Y, Murahashi Y, Takada Y, Mizutani-Koseki Y, Koseki H (2005) Mammalian polyhomeotic homologues Phc2 and Phc1 act in synergy to mediate polycomb repression of Hox genes. *Mol Cell Biol* **25:** 6694–6706

Ito K, Hirao A, Arai F, Takubo K, Matsuoka S, Miyamoto K, Ohmura M, Naka K, Hosokawa K, Ikeda Y, Suda T (2006) Reactive oxygen species act through p38 MAPK to limit the lifespan of hematopoietic stem cells. *Nat Med* **12:** 446–451

Iwama A, Oguro H, Negishi M, Kato Y, Morita Y, Tsukui H, Ema H, Kamijo T, Katoh-Fukui Y, Koseki H, van Lohuizen M, Nakauchi H (2004) Enhanced self-renewal of hematopoietic stem cells mediated by the polycomb gene product Bmi-1. *Immunity* **21:** 843–851

Jacobs JJ, Kieboom K, Marino S, DePinho RA, van Lohuizen M (1999) The oncogene and Polycomb-group gene bmi-1 regulates cell proliferation and senescence through the ink4a locus. *Nature* **397:** 164–168

Jagavelu K, Tietge UJ, Gaestel M, Drexler H, Schieffer B, Bavendiek U (2007) Systemic deficiency of the MAP kinase activated protein kinase 2 reduces atherosclerosis in hypercholesterolemic mice. *Circ Res* **101:** 1104–1112

Kiel MJ, Yilmaz OH, Iwashita T, Terhorst C, Morrison SJ (2005) SLAM family receptors distinguish hematopoietic stem and progenitor cells and reveal endothelial niches for stem cells. *Cell* **121:** 1109–1121

Kirito K, Fox N, Kaushansky K (2003) Thrombopoietin stimulates Hoxb4 expression: an explanation for the favorable effects of TPO on hematopoietic stem cells. *Blood* **102:** 3172–3178

Kotlyarov A, Neininger A, Schubert C, Eckert R, Birchmeier C, Volk HD, Gaestel M (1999) MAPKAP kinase 2 is essential for LPS-induced TNF-alpha biosynthesis. *Nat Cell Biol* **1:** 94–97

Kotlyarov A, Yannoni Y, Fritz S, Laass K, Telliez JB, Pitman D, Lin LL, Gaestel M (2002) Distinct cellular functions of MK2. *Mol Cell Biol* **22:** 4827–4835

Lessard J, Sauvageau G (2003) Bmi-1 determines the proliferative capacity of normal and leukaemic stem cells. *Nature* **423:** 255–260

Levine SS, King IF, Kingston RE (2004) Division of labor in polycomb group repression. *Trends Biochem Sci* **29:** 478–485

Lukas SM, Kroe RR, Wildeson J, Peet GW, Frego L, Davidson W, Ingraham RH, Pargellis CA, Labadia ME, Werneburg BG (2004) Catalysis and function of the p38 alpha.MK2a signaling complex. *Biochemistry* **43:** 9950–9960

Lund AH, van Lohuizen M (2004) Polycomb complexes and silencing mechanisms. *Curr Opin Cell Biol* **16:** 239–246

Molofsky AV, Pardal R, Iwashita T, Park IK, Clarke MF, Morrison SJ (2003) Bmi-1 dependence distinguishes neural stem cell self-renewal from progenitor proliferation. *Nature* **425:** 962–967

Neininger A, Kontoyiannis D, Kotlyarov A, Winzen R, Eckert R, Volk HD, Holtmann H, Kollias G, Gaestel M (2002) MK2 targets AU-rich elements and regulates biosynthesis of tumor necrosis factor and interleukin-6 independently at different post-transcriptional levels. *J Biol Chem* **277:** 3065–3068

Neininger A, Thielemann H, Gaestel M (2001) FRET-based detection of different conformations of MK2. *EMBO Rep* **2:** 703–708

Ohta H, Sawada A, Kim JY, Tokimasa S, Nishiguchi S, Humphries RK, Hara J, Takihara Y (2002) Polycomb group gene rae28 is required for sustaining activity of hematopoietic stem cells. *J Exp Med* **195:** 759–770

Park IK, Qian D, Kiel M, Becker MW, Pihalja M, Weissman IL, Morrison SJ, Clarke MF (2003) Bmi-1 is required for maintenance of adult self-renewing haematopoietic stem cells. *Nature* **423:** 302–305

Passegue E (2005) Hematopoietic stem cells, leukemic stem cells and chronic myelogenous leukemia. *Cell Cycle* **4:** 266–268

Platanias LC (2003) Map kinase signaling pathways and hematologic malignancies. *Blood* **101:** 4667–4679

Pokholok DK, Zeitlinger J, Hannett NM, Reynolds DB, Young RA (2006) Activated signal transduction kinases frequently occupy target genes. *Science* **313:** 533–536

Proft M, Mas G, de Nadal E, Vendrell A, Noriega N, Struhl K, Posas F (2006) The stress-activated Hog1 kinase is a selective transcriptional elongation factor for genes responding to osmotic stress. *Mol Cell* **23:** 241–250

Qiao F, Bowie JU (2005) The many faces of SAM. *Sci STKE* **2005:** re7

Quelle DE, Zindy F, Ashmun RA, Sherr CJ (1995) Alternative reading frames of the INK4a tumor suppressor gene encode two unrelated proteins capable of inducing cell cycle arrest. *Cell* **83:** 993–1000

Raingeaud J, Whitmarsh AJ, Barrett T, Derijard B, Davis RJ (1996) MKK3- and MKK6-regulated gene expression is mediated by the p38 mitogen-activated protein kinase signal transduction pathway. *Mol Cell Biol* **16:** 1247–1255

Rajasekhar VK, Begemann M (2007) Concise review: roles of polycomb group proteins in development and disease: a stem cell perspective. *Stem Cells* **25:** 2498–2510

Reya T, Duncan AW, Ailles L, Domen J, Scherer DC, Willert K, Hintz L, Nusse R, Weissman IL (2003) A role for Wnt signalling in self-renewal of haematopoietic stem cells. *Nature* **423:** 409–414

Ronkina N, Kotlyarov A, Dittrich-Breiholz O, Kracht M, Hitti E, Milarski K, Askew R, Marusic S, Lin LL, Gaestel M, Telliez JB (2007) The mitogen-activated protein kinase (MAPK)-activated protein kinases MK2 and MK3 cooperate in stimulation of tumor necrosis factor biosynthesis and stabilization of p38 MAPK. *Mol Cell Biol* **27:** 170–181

Schumacher S, Laass K, Kant S, Shi Y, Visel A, Gruber AD, Kotlyarov A, Gaestel M (2004) Scaffolding by ERK3 regulates MK5 in development. *EMBO J* **23:** 4770–4779

Stokoe D, Engel K, Campbell DG, Cohen P, Gaestel M (1992) Identification of MAPKAP kinase 2 as a major enzyme responsible for the phosphorylation of the small mammalian heat shock proteins. *FEBS Lett* **313:** 307–313

Suda T, Arai F, Hirao A (2005) Hematopoietic stem cells and their niche. *Trends Immunol* **26:** 426–433

Suzuki M, Mizutani-Koseki Y, Fujimura Y, Miyagishima H, Kaneko T, Takada Y, Akasaka T, Tanzawa H, Takihara Y, Nakano M, Masumoto H, Vidal M, Isono K, Koseki H (2002) Involvement of the Polycomb-group gene Ring1B in the specification of the anterior-posterior axis in mice. *Development* **129:** 4171–4183

Tamura K, Sudo T, Senftleben U, Dadak AM, Johnson R, Karin M (2000) Requirement for p38alpha in erythropoietin expression: a role for stress kinases in erythropoiesis. *Cell* **102:** 221–231

Tanoue T, Adachi M, Moriguchi T, Nishida E (2000) A conserved docking motif in MAP kinases common to substrates, activators and regulators. *Nat Cell Biol* **2:** 110–116

Valk-Lingbeek ME, Bruggeman SW, van Lohuizen M (2004) Stem cells and cancer; the polycomb connection. *Cell* **118:** 409–418

van der Lugt NM, Domen J, Linders K, van Roon M, Robanus-Maandag E, te Riele H, van der Valk M, Deschamps J, Sofroniew M, van Lohuizen M, Berns A (1994) Posterior transformation, neurological abnormalities, and severe hematopoietic defects in mice with a targeted deletion of the bmi-1 proto-oncogene. *Genes Dev* **8:** 757–769

Vertii A, Hakim C, Kotlyarov A, Gaestel M (2006) Analysis of properties of small heat shock protein Hsp25 in MAPK-activated protein kinase 2 (MK2)-deficient cells: MK2-dependent insolubilization of Hsp25 oligomers correlates with susceptibility to stress. *J Biol Chem* **281:** 26966–26975

Voncken JW, Niessen H, Neufeld B, Rennefahrt U, Dahlmans V, Kubben N, Holzer B, Ludwig S, Rapp UR (2005) MAPKAP kinase 3pK phosphorylates and regulates chromatin association of the polycomb group protein Bmi1. *J Biol Chem* **280:** 5178–5187

White A, Pargellis CA, Studts JM, Werneburg BG, Farmer II BT (2007) Molecular basis of MAPK-activated protein kinase 2:p38 assembly. *Proc Natl Acad Sci USA* **104:** 6353–6358

Winzen R, Kracht M, Ritter B, Wilhelm A, Chen CY, Shyu AB, Muller M, Gaestel M, Resch K, Holtmann H (1999) The p38 MAP kinase pathway signals for cytokine-induced mRNA stabilization via MAP kinase-activated protein kinase 2 and an AU-rich region-targeted mechanism. *EMBO J* **18:** 4969–4980

Yamaki M, Isono K, Takada Y, Abe K, Akasaka T, Tanzawa H, Koseki H (2002) The mouse Edr2 (Mph2) gene has two forms of mRNA encoding 90- and 36-kDa polypeptides. *Gene* **288:** 103–110

Yannoni YM, Gaestel M, Lin LL (2004) P66(ShcA) interacts with MAPKAP kinase 2 and regulates its activity. *FEBS Lett* **564:** 205–211

Zhao M, New L, Kravchenko VV, Kato Y, Gram H, di Padova F, Olson EN, Ulevitch RJ, Han J (1999) Regulation of the MEF2 family of transcription factors by p38. *Mol Cell Biol* **19:** 21–30

Zink B, Paro R (1989) *In vivo* binding pattern of a trans-regulator of homoeotic genes in Drosophila melanogaster. *Nature* **337:** 468–471

STEM CELLS®
TISSUE-SPECIFIC STEM CELLS

Maintenance of Undifferentiated State and Self-Renewal of Embryonic Neural Stem Cells by Polycomb Protein Ring1B

MÓNICA ROMÁN-TRUFERO,[a] HÉCTOR R. MÉNDEZ-GÓMEZ,[b,c] CLAUDIA PÉREZ,[d] ATSUSHI HIJIKATA,[e] YU-ICHI FUJIMURA,[e] TAKAHO ENDO,[f] HARUHIKO KOSEKI,[e] CARLOS VICARIO-ABEJÓN,[b,c] MIGUEL VIDAL[a]

[a]Cell and Developmental Biology, Centro de Investigaciones Biológicas and [b]Molecular, Cellular and Developmental Neurobiology, Instituto Cajal, Consejo Superior de Investigaciones Cientificas (CSIC), Madrid, Spain; [c]Centro de Investigaciones Biomédicas en Red sobre Enfermedades Neurodegenerativas (CIBERNED), Instituto de Salud Carlos III, Madrid, Spain; [d]Anatomy and Histopathology, Facultad de Veterinaria, Universidad de León, Campus Vegazana, León, Spain; [e]Developmental Genetics and [f]Bioinformatics and Systems Engineering Division, RIKEN Research Center for Allergy and Immunology, Yokohama, Japan

Key Words. Ring1B • Polycomb • Stem cell • Neural differentiation • Self-renewal

ABSTRACT

Cell lineages generated during development and tissue maintenance are derived from self-renewing stem cells by differentiation of their committed progeny. Recent studies suggest that epigenetic mechanisms, and in particular the Polycomb group (PcG) of genes, play important roles in controlling stem cell self-renewal. Here, we address PcG regulation of stem cell self-renewal and differentiation through inactivation of Ring1B, a histone H2A E3 monoubiquitin ligase, in embryonic neural stem cells (NSCs) from the olfactory bulb of a conditional mouse mutant line. We show that neural stem/progenitor cell proliferation in vivo and in neurosphere assays is impaired, lacking Ring1B, and their self-renewal and multipotential abilities, assessed as sphere formation and differentiation from single cells, are severely affected. We also observed unscheduled neuronal, but not glial, differentiation of mutant stem/progenitor cells under proliferating conditions, an alteration enhanced in cells also lacking Ring1A, the Ring1B paralog, some of which turned into morphologically identifiable neurons. mRNA analysis of mutant cells showed upregulation of some neuronal differentiation–related transcription factors and the cell proliferation inhibitor Cdkn1a/p21, as well as downregulation of effectors of the Notch signaling pathway, a known inhibitor of neuronal differentiation of stem/progenitor cells. In addition, differentiation studies of Ring1B-deficient progenitors showed decreased oligodendrocyte formation in vitro and enhanced neurogenesis and reduced gliogenesis in vivo. These data suggest a role for Ring1B in maintenance of the undifferentiated state of embryonic neural stem/progenitor cells. They also suggest that Ring1B may modulate the differentiation potential of NSCs to neurons and glia. STEM CELLS *2009;27:1559–1570*

Disclosure of potential conflicts of interest is found at the end of this article.

INTRODUCTION

The generation of cell lineages during development and the integrity of tissues in the adult depends on a variety of self-renewing embryonic and adult stem cells [1]. Self-renewal allows the maintenance of pools of stem cells needed for appropriate embryo development and cell replacement during an organism's life span [2]. Stem cell self-renewal combines the ability to proliferate with the preservation of developmental potential [3]. Embryonic stem (ES) and fetal stem cells proliferate extensively, in contrast to adult stem cells, which proliferate rather sparsely and rely on transit-amplifying progenitors for cell expansion [1, 4]. Developmental potential is maximal in ES cells (pluripotent), whereas other embryonic/fetal and adult stem cells show lineage-restricted potential [1, 5].

Studies on ES cells show that self-renewal is determined by a regulatory network of transcription factors acting together with chromatin regulators, thus defining a cell type–specific epigenetic landscape [6–9]. Among epigenetic regulators, the Polycomb group (PcG) of genes encodes subunits of chromatin complexes (Polycomb repressing complexes [PRCs]). Two of these subunits are endowed with chromatin-

Author contributions: M.R.-T.: collection and/or assembly of data, data analysis and interpretation; H.M.-G.: collection and/or assembly of data, data analysis; C.P.: collection and assembly of data; A.H.: data analysis; Y.F.: collection and assembly of data; T.E.: data analysis; H.K.: provision of study material or patients; C.V.-A.: conception and design, data analysis and interpretation, manuscript revision, financial support; M.V.: conception and design, data analysis and interpretation, financial support, manuscript writing and final approval of manuscript; C.V.-A. and M.V. contributed equally to this work.

Correspondence: Miguel Vidal, Ph.D., Cell and Developmental Biology, Centro de Investigaciones Biológicas, CSIC, Ramiro de Maeztu 9, 28040 Madrid, Spain. Telephone: 34 918373112; Fax: 34 915360432; e-mail: mvidal@cib.csic.es; or Carlos Vicario-Abejón, Ph.D., Molecular, Cellular and Developmental Neurobiology, Instituto Cajal, CSIC, Avda. Doctor Arce 37, 28002 Madrid, Spain. Telephone: 34 915854721; Fax: 34 915854754; e-mail: cvicario@cajal.csic.es Received August 6, 2008; accepted for publication March 12, 2009; first published online in STEM CELLS *EXPRESS* April 2, 2009. 1066-5099/2009/$30.00/0 doi: 10.1002/stem.82

modifying activities. One, Ezh2, is a methyltransferase that modifies lysine 27 of histone H3 [10], whereas Ring1B and its paralog Ring1A are E3 monoubiquitin ligase that modify lysine 119 of histone H2A [11]. Both enzymatic activities belong in nonoverlapping core protein complexes unique to a variety of biochemical entities grouped as PRC2 (H3K27 methyltransferase) and PRC1 (H2AK119 monoubiquitin ligase) [12]. These histone modifications are commonly found on transcriptionally silent loci [13–16]. Currently, it is accepted that PRC2 acts as an instructed chromatin-modifying module [17], whereas PRC1 acts as a reader device that binds to H3K27 methylated nucleosomes [10, 18], although sometimes PRC1 subunits are also recruited to chromatin in a H3K27-independent manner [19].

The PcG role in stem cell self-renewal is best known for ES cells and hematopoietic stem cells [20]. In ES cells, PcG products act as repressors of transcription factors and of components of signaling modules widely used in the generation of cell lineages that appear during development [13, 15]. Recently, it was shown that PRC2-dependent markers and other epigenetic markers are related to changing transcriptional programs associated with transitions from ES cell–derived neural stem cells (NSCs) to neural progenitors and their differentiated progeny [21]. The impact of PcG regulation on NSC self-renewal is more limited and is derive mostly from the study of loss-of-function models of Pcgf4/Bmi1, a PRC1 subunit that acts as a cofactor in H2A ubiquitylation by Ring1A/Ring1B [22]. Mice lacking Bmi1 have a lower number of adult NSCs whose self-renewal ability is severely impaired [23–25]. Acute inactivation of Bmi1, by short hairpin (sh)RNA-mediated inactivation of embryonic neural stem/progenitor cells also results in defective self-renewal [26]. Both Bmi1-deficient adult and fetal stem/progenitor cells have upregulated inhibitors of cell cycle progression. Although Ring1B and Bmi1 are part of a common regulatory device [22, 27], they also show distinctive activities, as seen, for example, in the adult hematopoietic compartment [28]. Here, we set out to investigate the role of the PcG histone E3 monoubiquitin ligase Ring1B in the self-renewal and differentiation potential of embryonic NSCs. Using a model of conditional inactivation of Ring1B to study self-renewal of NSCs from the fetal olfactory bulb, we show that Ring1B promotes embryonic NSC self-renewal by sustaining their proliferative activity and maintaining their undifferentiated state and developmental potential.

Materials and Methods

Mice

Ring1B conditional knockout, *Ring1A* knockout, and genotyping were described previously [28, 29]. Inducible Cre-expressing mouse lines were *Polr2a::CreERT2* [30] and *Rosa26:CreERT2* [31]. Animal handling procedures were institutionally approved and were in accordance with national and European regulations.

Neural Stem/Progenitor Cell Culture

Reagents for cell cultures were bought from Invitrogen (Carlsbad, CA, http://www.invitrogen.com), Sigma-Aldrich (St. Louis, MO, http://www.sigmaaldrich.com), and PeproTech (Rocky Hill, NJ, http://www.peprotech.com). Embryonic olfactory bulb stem cells (OBSCs) were prepared from the olfactory bulb of 13.5 days postcoitum (dpc) mice. Cells were plated and expanded in Dulbecco's modified Eagle's medium (DMEM)/nutrient mixture F12/insulin, apotransferrin, putrescine, progesterone, and sodium selenite supplemented with fibroblast growth factor (FGF)-2 and epidermal growth factor (EGF) [32]. Proliferation assays were performed in cells growing in the presence of FGF-2 and EGF. Cultures were pulsed with 5′-bromo-2-deoxyuridine (BrdU) for 1 hour before fixation. Differentiation assays were performed after mitogen removal from the cultures. For clonal analysis, OBSC spheres were dissociated into a single-cell suspension and diluted to eight cells/ml in DMEM/F12/N12:OBSC-conditioned medium (1:1). Two hundred μl of this suspension was plated into each well of 96-well plates. One day after seeding, wells containing a single cell were marked and induced to proliferate for 9 days, when the wells were screened for the presence of clonal neurospheres. Differentiated clonally derived secondary spheres were finally fixed and triple immunostained to detect the presence of neurons, astrocytes, and oligodendrocytes [33].

Immunostaining of Cultured Cells

Cells were fixed in 4% paraformaldehyde (PFA) and incubated with antibodies to: Ring1B (1:250 [34]), β-tubulin III (Tuj1, 1:2,000; Covance, Princeton, NJ, http://www.covance.com), glial fibrillary acidic protein (GFAP, 1:800; Millipore, Billerica, MA, http://www.millipore.com), O4 (1:8), microtubule-associated protein 2ab (Map2ab) (1:250; Sigma), neurofilament medium chain (NF-m) (1:400; Encor Biotechnology, Gainesville, FL, http://www.encorbio.com), and BrdU (1:1,000; Becton, Dickinson and Company, Franklin Lakes, NJ, http://www.bd.com). Differentiated clones were triple immunostained with antibodies against β-tubulin III (rabbit antibody diluted 1:2,000; Covance), GFAP (mouse antibody, diluted 1:800; Millipore), and O4 (diluted 1:8). The O4 antibody was obtained from the culture medium of O4-producing hybridoma cells, kindly provided by A. Rodríguez-Peña, Consejo Superior de Investigaciones Cientificas. Appropriate secondary antibodies were used to detect specific signals. Cultures were stained with 2 μg/ml 4′,6-diamino-2-phenylindole (DAPI) to stain the nuclei and allow total cell counting.

A terminal deoxynucleotidyl transferase dUTP nick end labeling (TUNEL) assay was performed following the manufacturer's instructions (Roche Diagnostics, Basel, Switzerland, http://www.roche-applied-science.com).

Immunostaining of Tissue Sections

Embryonic day (E)17.5 mouse embryos were perfused with 4% PFA and embryo heads were postfixed in 4% PFA for 2 hours, cryoprotected with Tissue-Tek (Sakura, Tokyo, Japan, http://www.sakura.com), and then frozen at −80°C. Coronal cryostat sections (14 μm) were immunostained with antibodies against: Ring1B (1:400), phospho-H3 (PH3, 1:1,000; Millipore), Tuj1 (1:2,000), GFAP (1:800), and nestin (mouse monoclonal diluted 1:50; Millipore). The TUNEL assay (Roche's kit) was also performed on cryostat sections. Ring1B and Tuj1 immunohistochemistry was done on 7-μm sections of paraffin-embedded fixed embryos. Binding of anti-Ring1B [34] and anti-Tuj1 antibodies was detected with the avidin–biotin–peroxidase complex method (Peroxidase Elite, Vectastain, and ABC kit; Vector Laboratories, Burlingame, CA, http://www.vectorlabs.com) followed by counterstaining with hematoxylin-eosin. Cryostat sections were also prepared from the OBs of E17.5 embryos from pregnant mice that were injected i.p. with BrdU (100 μg/g) 4 hours before embryos were removed. Sections were double immunostained with antibodies against BrdU (1:200; Abcam, Cambridge, U.K., http://www.abcam.com) and Tuj1 or nestin (rabbit polyclonal, diluted 1:1,000, provided by R. McKay, NIH), followed by appropriate fluorescent secondary antibodies. Some sections were stained with DAPI.

Western Blot Analysis

Cells were lysed in RIPA buffer (10 mM Tris-HCl, pH 7.2; 150 mM NaCl; 1% Triton-100; 0.1% sodium dodecyl sulfate; 1% sodium deoxycholate; 5 mM EDTA, 20 mM NaF and Complete [Roche]). Thirty-five μg of total extract was subjected to SDS-PAGE electrophoresis and posterior immunoblotting following standard procedures. Nitrocellulose membranes were incubated

with antibodies specific for Ring1B [34] and α-tubulin (Sigma, clone B-5-1-2).

Microarray Methods and Gene Ontology Analysis

Total RNA was extracted using the Trizol reagent (Invitrogen) and purified with Qiagen RNeasy separation columns (Qiagen, Hilden, Germany, http://www1.qiagen.com). First-strand cDNA was synthesized and hybridized to Affymetrix GeneChip Mouse Genome 430 2.0 arrays (Affymetrix, Santa Clara, CA, http://www.affymetrix.com) to assess and compare the overall gene expression profiles. The signal intensities of probe sets in each chip were normalized with the gcRMA algorithm [35] implemented in the Bioconductor package (Bioconductor, http://bioconductor.org) to estimate the expression value of each probe set in the chip. The annotation information for the probe sets was obtained from RefDIC (RIKEN Research Center for Allergy and Immunology, http://refdic.rcai.riken.jp) [36], and probe sets having no gene information or matching two or more genes were excluded from the analysis. We considered only probe sets whose expression values varied by twofold or more between Ring1B-deficient cells and control cultures. For 972 up/downregulated genes, gene ontology (GO) term enrichment analysis was performed according to a method described by Draghici et al. [37], with a correction for multiple testing using the false discovery rate (FDR) [38]. Eventually, GO terms with a FDR < 0.05 were selected as functionally enriched terms.

Quantitative Reverse Transcription-Polymerase Chain Reaction

Total RNA was isolated using Trizol (Invitrogen) and the reverse transcription (RT) reaction was carried out using the First Strand Synthesis Kit according to the manufacturer's guidelines (Invitrogen). A quantitative polymerase chain reaction (QPCR) analysis was performed in triplicate using 150 ng cDNA per reaction in an iQ5 with Bio-Rad SYBR-Green (Bio-Rad, Hercules, CA, http://www.bio-rad.com). Gene expression data were analyzed with iQ5 software (Bio-Rad). Sequences of primer pairs for the QPCR were obtained from the Primer Bank [39]: *Hes1*, 6680205a2; *Hes5*, 6754182a1; *Hey1*, 6754188a1; *NeuroD1*, 33563268a1; *Tubb3*, 12963615a1; *Cdkn1a*, 6671726a3; *Ina*, 34328368a1; *Id4*, 13624309a1; *Eomes/Tbr2*, 5738950a1; *Prdm16*, 33186878a2; *Ascl1*, 6678806a1; *Zfhx3/Athf1*, 6680736a1; *Nr2f2/COUP-TFII*, 6753104a1. Other primers were: *Cdkn2a*, 5′-CGAACTCTTTCGGTCGTACCC-3′(forward) and 5′-CGAATCTGCACCGTAGTTGAGC-3′ (reverse) and *Cdknd*, 5′-CTGAACCGCTTTGGCAAGAC-3′ (forward) and 5′-GCCCTCTCTTATCGCCAGAT-3′ (reverse).

Cell Counts and Statistical Analysis

To determine the number of cultured cells expressing a specific antigen, 10 random fields were counted per coverslip using a 40× objective and fluorescence filters [33]. $PH3^+$ cells and $GFAP^+$ cells were counted in 24 serially cut cryostat sections ($n = 3$ wild-type mice and $n = 3$ $Ring1B^{\Delta/\Delta}$ mice). To count $BrdU^+$ and $TuJ1^+$ cells, confocal images from cryostat sections were taken every micron. The entire image stacks were then analyzed and the cells were counted using ImageJ software (Wayne Rasband, National Institutes of Health, USA). Statistical analysis was performed using Student's *t*-test and Sigma Stat Software (Sigma).

Results

Ring1B Is Required for Proliferation of NSCs

Multipotent self-renewing NSCs can be propagated in cell suspension cultures, where they form cell aggregates known as neurospheres [40]. Under these conditions, survival and expansion of stem and progenitor cells result in populations of undifferentiated cells that retain their ability to differentiate in vitro to neuronal and glial derivatives. Typically, neurosphere cultures are established from embryonic brain regions or from the adult subventricular zone and the OB [31, 41]. To investigate the role of Ring1B in NSC self-renewal, we isolated cells from the embryonic OB that are known to show multipotential and self-renewing capacities under clonal analysis conditions. These cells reside in the proliferating layers (neuroepithelial zone) of the OB and express Ring1B (Fig. 1A). We dissected the OB from 13.5 dpc fetuses homozygous for a floxed Ring1B (*Ring1B^f*) allele that can be inactivated by Cre-mediated recombination, a strategy needed to circumvent the embryonic lethality of Ring1B inactivation [28, 42]. This *Ring1B* mutant allele was obtained by homologous recombination of a targeting construct in which *loxP* sequences flank the first coding exon of the *Ring1B* gene and a selectable *neo* cassette (Fig. 1B) [28]. These fetuses also ubiquitously expressed a cytoplasmic Cre recombinase–estrogen receptor fusion protein (Cre-ERT2) whose activity is controlled by translocation to the cell nucleus induced by 4-hydroxy-tamoxifen (4HT) [43] (Fig. 1B). NSCs were expanded in the presence of growth factors, EGF and FGF-2, and cultured in neurosphere-forming conditions, as previously described [33]. To obtain Ring1B-deficient progenitors, we treated parallel cultures seeded at 5,000 cells/cm^2 with 800 nM 4HT in ethanol, or with only vehicle, for 18 hours and scored the resulting neurospheres 72 hours later. At this stage, 4HT treatment resulted in Ring1B-depleted cell cultures, as shown by Western blot and Ring1B immunofluorescence analysis (Fig. 1C, supporting information Fig. 1A). We termed

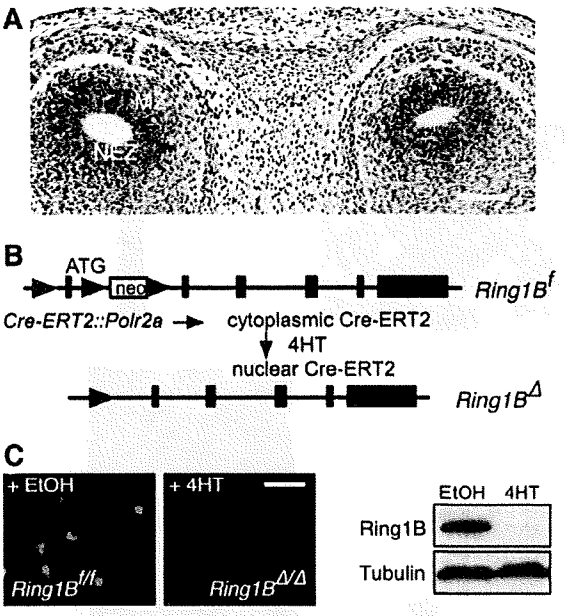

Figure 1. Ring1B expression in the fetal olfactory bulb and strategy for Ring1B inactivation in olfactory bulb stem cells (OBSCs). **(A):** Histochemical analysis of 13.5 days postcoitum olfactory bulb, showing high levels of Ring1B in the neuroepithelial zone (NEZ); some cells located in the mantle zone (MZ) also expressed Ring1B. **(B):** Strategy for generation of *Ring1B$^{\Delta/\Delta}$* cells. ATG denotes the initiation codon of Ring1B, red triangles loxP sequences and filled boxes Ring1B exons. **(C):** Ring1B immunostaining (left) and Western blotting (right) analysis of control OBSCs (ethanol [EtOH]) and *Ring1B$^{\Delta/\Delta}$* OBSCs (hydroxytamoxifen, [+4HT]) shows almost total deletion of Ring1B 4 days after treatment under proliferation conditions (<5% of cells were immunoreactive for Ring1B). Scale bars = 100 microns **(A)**, 45 microns **(C)**.

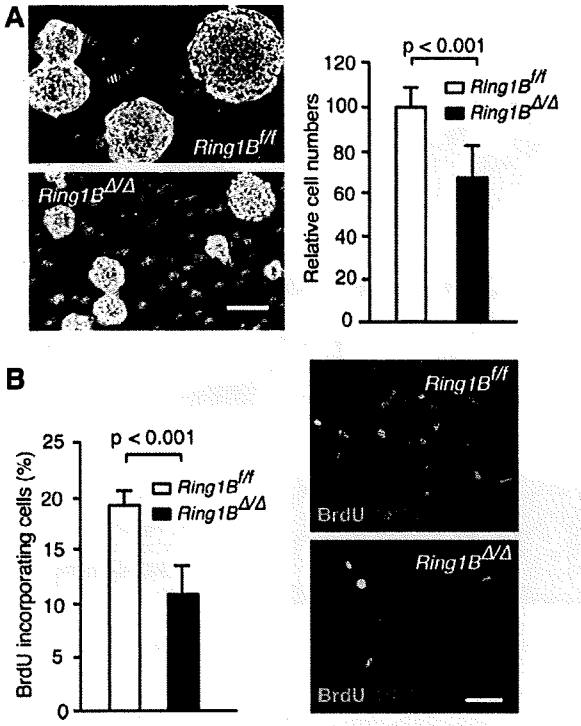

Figure 2. Impaired proliferation of *Ring1B* mutant olfactory bulb stem cells in neurosphere assays. **(A):** *Ring1B* mutant cultures show less sphere formation (left) and a lower total number of cells (right, $n = 24$). **(B):** The number of cells incorporating 5′-bromo-2-deoxyuridine (BrdU) (left, $n = 7$), as assessed by immunofluorescence analysis (right), was significantly lower in $Ring1B^{\Delta/\Delta}$ cultures than in control cultures. Error bars depict the standard error of the mean. Scale bar = 100 microns **(A)**, 45 microns **(B)**.

4HT-treated and ethanol-treated cultures as $Ring1B^{\Delta/\Delta}$ and $Ring1B^{f/f}$, respectively. $Ring1B^{\Delta/\Delta}$ cultures consisted of neurospheres whose size was smaller than that of wild-type neurospheres (Fig. 2A, left, and also the clonal analysis in Fig. 3). This observation was consistent with a poorer expansion of Ring1B-deficient cells, as indicated by the total number of cells in mutant versus wild-type cultures under proliferating conditions (Fig. 2A, right). To eliminate the possibility that transient nuclear activity of the recombinase Cre had a toxic effect on cell growth, we characterized the proliferative properties of neurospheres derived from *Cre-ERT2::Polr2a* mice and found that the proportion of BrdU-incorporating cells in tamoxifen-treated cultures was similar to that in control, ethanol-treated cultures (supporting information Fig. 1B). We also investigated the possible role of 4HT treatment characterizing neurosphere cultures from OB cells isolated from wild-type mice and found them to be indistinguishable from vehicle-treated neurospheres in cell proliferation assays (supporting information Fig. 1C). Thus, these experimental conditions had no effect on the observed results and, therefore, we conclude that the appropriate proliferation of neural stem/progenitors depends, in a cell-autonomous manner, on the activity of *Ring1B*. We then studied whether the decrease in cell numbers in mutant cultures was due to differences in apoptosis or in proliferative rates. The TUNEL analysis showed almost no apoptotic cells in either culture (0.3% and 0.2% of total cells in $Ring1B^{\Delta/\Delta}$ cultures and wild-type cultures, respectively; data not shown). In contrast, quantitation cultures that were BrdU pulsed for 1 hour demonstrated that 4HT-treated cultures contained fewer cells that had incorporated BrdU (19%) than cultures treated with ethanol (12%; $p < .005$) (Fig. 2B). To see whether this observation on OB-derived NSCs could be generalized to NSCs from other regions of the central nervous system, we investigated the proliferative properties of neurospheres derived from the cortex and ganglionic eminences of 13.5 dpc embryos. The results (supporting information Fig. 2) showed that, in the absence of Ring1B, neurosphere formation and proliferation, assessed as BrdU incorporation, were lower than in $Ring1B^{f/f}$ cultures. Collectively, these results show that defective expansion of mutant neural stem/progenitors results from a decrease in the proliferative rate of Ring1B-deficient cells.

Defective Self-Renewal of Ring1B-Deficient NSCs

The nonclonal neurosphere assay assesses the presence of NSCs but it does not inform on their self-renewal capacity. Instead, self-renewal is usually analyzed by the ability of single cells to reform spheres while retaining the production of neurons and glia. To determine whether Ring1B plays a role in NSC self-renewal, we quantitated the number of cells able to reform neurospheres when cultured as single cells. First, we treated single cell cultures with 4HT and cultured them for 7-9 days to obtain primary $Ring1B^{\Delta/\Delta}$ neurospheres (Fig. 3A, top). Efficient inactivation of Ring1B in these cultures was assessed by PCR analysis of single spheres (supporting information Fig. 3A). Second, we set up single-cell cultures from neurospheres derived from Ring1B-deficient cells to derive mutant secondary neurospheres (Fig. 3A, bottom). We also tried to establish neurospheres from two stages of single-cell cultures, but under these conditions no neurospheres were obtained from mutant OBSCs (supporting information 3B, 3C). The assays revealed that the capacity of $Ring1B^{\Delta/\Delta}$ cells to give rise to primary neurospheres was one third lower ($p < .001$) than that of wild-type cells, and that such a capacity was further reduced in secondary neurospheres, to only one fifth of that of wild-type cells ($p < .001$) (Fig. 3B). Sizes of primary and secondary mutant neurospheres from the clonal analysis were, as already seen in nonclonal neurosphere assays, smaller than those of wild-type cells (46% and 63% of that of wild-type spheres) (Fig. 3D, 3E). The comparison of neurosphere sizes obtained in these clonal assays showed a distinctive distribution in which wild-type cells generated neurospheres in the range of 200-1,800 microns in diameter, whereas mutant cells never reached diameters >800 microns (Fig. 3C). Altogether, the data show that Ring1B is required for self-renewal and proliferation of OB stem cells.

Premature Differentiation of Ring1B-Deficient NSCs

To address whether the impaired proliferation and self-renewal abilities of mutant NSCs is related to Ring1B regulation of differentiation, we evaluated the potential of E13.5-derived OB neurospheres to generate the three major neural cell lineages normally found when they are cultured under differentiation conditions, without mitogens. We found that both Ring1B-deficient and wild-type cultures formed similar numbers of neurons (Tuj1 immunoreactive cells) and astrocytes (GFAP immunoreactive cells), as shown in Figure 4. In contrast, we found a consistently lower number of oligodendrocytes (O4 immunoreactive cells) in cultures that lacked Ring1B. We tested the possibility that mutant cells were counterselected during their time in culture by identifying Ring1B-expressing cells with anti-Ring1B antibodies in cultures undergoing differentiation. The results (supporting information Fig. 4A) showed that, whereas all cells in control

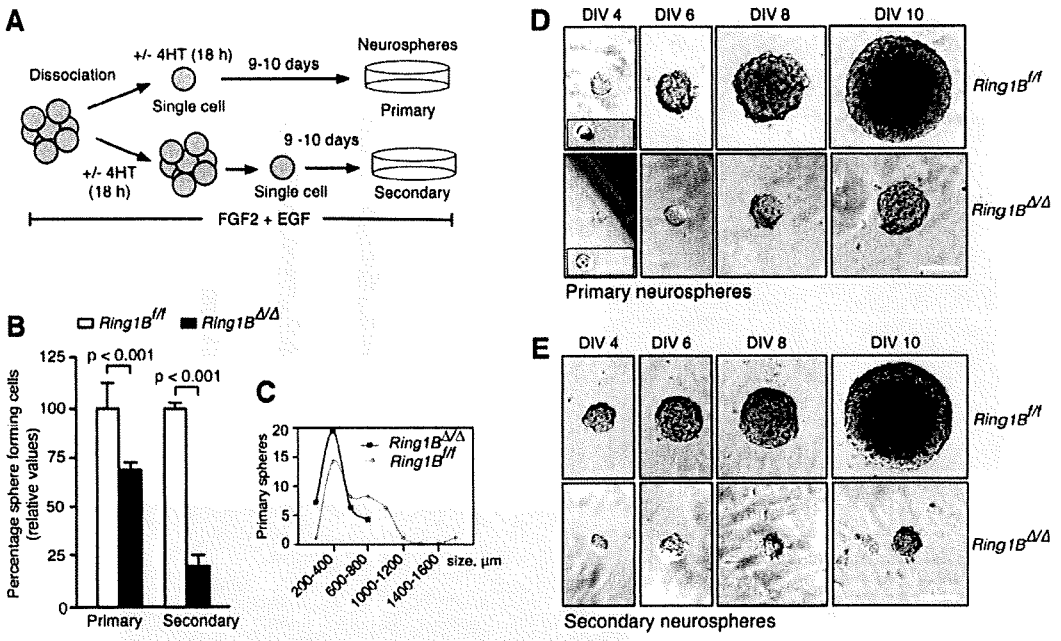

Figure 3. Ring1B deletion reduces the self-renewal capacity of olfactory bulb stem cells. **(A):** Schematic diagram of clonal analysis protocols to obtain primary and secondary $Ring1B^{\Delta/\Delta}$ spheres. In the first protocol (upper), 4-hydroxy-tamoxifen (4HT) was added to the cultures 18 hours before plating single cells and sphere formation was scored after 9 days in culture. In the second protocol (bottom), 4HT was added at the time of plating cells at a density of 5,000 cells/cm^2, to allow the formation of $Ring1B^{\Delta/\Delta}$ primary spheres. Four days after 4HT addition, primary spheres were disaggregated and plated as single cells. $Ring1B^{\Delta/\Delta}$ secondary sphere formation was also scored after 9 days in culture. **(B):** The percentages of single cells forming primary and secondary spheres were significantly lower, by 28% ($n = 3$ experiments; $p < .001$) and 75% ($n = 2$ experiments; $p < .001$), respectively, in $Ring1B$ mutant cultures. **(C):** Distribution of the number of primary $Ring1B^{\Delta/\Delta}$ neurospheres versus their diameter, showing that, in mutant cultures, most spheres were smaller in size compared with controls. After 9 days in culture, the average sizes of primary spheres were 602.6 ± 54.5 microns and 326.6 ± 24.2 microns for control and $Ring1B^{\Delta/\Delta}$ cultures, respectively; for secondary spheres, values of average sizes were 725.3 ± 51.2 microns and 271.2 ± 32.3 microns for the control and mutant cultures, respectively. Total numbers of clonal spheres analyzed were 83 primary and 44 secondary control spheres and 70 primary and 12 secondary $Ring1B^{\Delta/\Delta}$ spheres. **(D, E):** Primary and secondary neurosphere cultures showing representative spheres throughout the indicated times in culture (DIV, days in vitro) after seeding single cells (inset). Scale bar for single cells, 25 microns; clonal spheres, 80 microns. Error bars depict the standard error of the mean.

cultures were stained for Ring1B. 4HT-treated cultures lacked Ring1B immunoreactivity. Because the differentiation potential of NSCs can change with developmental time, we also addressed the phenotype of neurospheres derived from 18.5 dpc OBs. Similarly to observations for Ring1B-deficient 13.5 dpc NSCs, mutant 18.5 dpc OBSCs showed impaired neurosphere formation and decreased proliferation (supporting information Fig. 5A), compared with that of untreated cultures. In the absence of growth factors, both 4HT-treated or untreated cultures generated similar proportions of the three cell lineages, although a (statistically not significant) trend toward a lower number of oligodendrocytes was observed for $Ring1B^{\Delta/\Delta}$ cultures (supporting information Fig. 5B). Considering that most differentiated derivatives from wild-type cells are neurons and astrocytes, the overall differentiating potential of Ring1B-deficient cells growing under nonclonal conditions was similar to that of $Ring1B^{f/f}$ cells after induction of differentiation. To better ascertain the differentiation potential of mutant stem cells, single cell–derived neurospheres were induced to differentiate, revealing a lower (30% of that of $Ring1B^{f/f}$ cells) number of tripotent clonal neurospheres (Fig. 4C, 4D). Also, the overall differentiation potential of mutant clonally derived neurospheres was lower (50% of that of $Ring1B^{f/f}$ cells).These findings unveil a defective differentiation potential of $Ring1B^{\Delta/\Delta}$ OBSCs that was masked under nonclonally derived neurospheres in nonclonal neurosphere cultures.

We next asked whether Ring1B might play a role in maintaining neural stem/progenitor cells undifferentiated, as has been observed in ES cells [15, 44]. To this end, we analyzed 4HT-treated and untreated OB stem cell cultures growing in the presence of mitogens for the expression of the neuronal differentiation marker β-tubulin III (Tuj1). We found that $Ring1B^{\Delta/\Delta}$ cultures contained a larger fraction (13%) of immunoreactive cells than wild-type cultures (1.4%) (Fig. 5A), suggesting that Ring1B deficiency leads to a weakened stability of the undifferentiated state of mutant cells. If, indeed, Ring1B is playing a role in the maintenance of the undifferentiated state, we reasoned that a differentiated phenotype would be better observed in stem/progenitor cells derived from compound mutant embryos in which both $Ring1B$ and its paralog $Ring1A$ are inactivated. Figure 5B shows that more than one third of $Ring1A^{-/-}Ring1B^{\Delta/\Delta}$ OB stem/progenitor cells growing in the presence of FGF and EGF-2 were immunoreactive for Tuj1, compared with <1% among those in single $Ring1A$ mutant cell cultures. In addition, examples of cells possessing clear neuronal morphologies could be seen among Ring1A- and Ring1B-lacking cultures (Fig. 5B, inset). This was corroborated by double immunostaining of TuJ1$^+$ cells with Map2ab or NF-m, neuronal markers that label dendrites

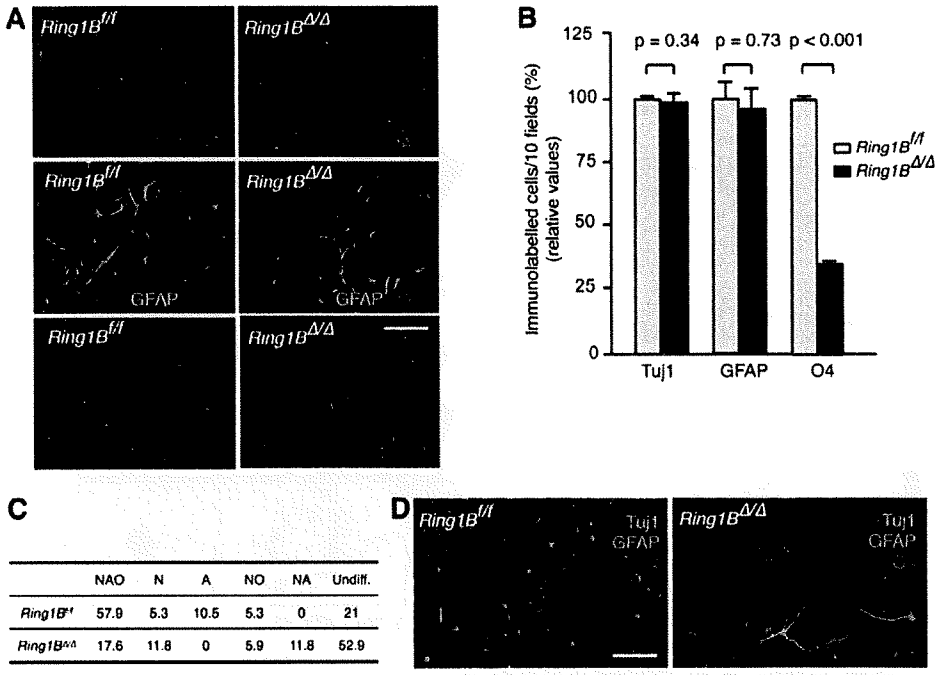

	NAO	N	A	NO	NA	Undiff.
Ring1B$^{f/f}$	57.9	5.3	10.5	5.3	0	21
Ring1B$^{Δ/Δ}$	17.6	11.8	0	5.9	11.8	52.9

Figure 4. Differentiation of olfactory bulb stem cells to neurons, astrocytes, and oligodendrocytes after mitogen removal. **(A):** Morphology and immunofluorescence analysis of differentiation markers in wild-type and Ring1B-deficient neural progenitors cultured for 4 days in the absence of growth factors. **(B):** Quantitation ($n = 6$) of cell lineages identified by Tuj1 (neurons), GFAP (astrocytes), and O4 (oligodendrocytes). Whereas the proportions of neurons and astrocytes were similar between wild-type and mutant cultures, Ring1B-deficient oligodendrocytes were found at a lower (one third) frequency than in wild-type cultures. Error bars depict the standard error of the mean. **(C):** Quantitation, as a percentage, of cell lineages identified in the differentiation of clonally derived neurospheres from control (20 clones) and mutant (17 clones) cultures showing tripotent (NAO), bipotent (NO, NA), and unipotent clones (N, A). **(D):** Morphology and immunofluorescence analysis of differentiation markers in representative tripotent clones of control and mutant cultures. Scale bars = 55 microns **(A)**, 50 microns **(D)**. Abbreviations: A, astrocytes; DAPI, 4′,6-diamino-2-phenylindole; GFAP, glial fibrillary acidic protein; N, neurons; O, oligodendrocytes; undiff., clones that did not express any of the differentiation markers.

and axons, respectively (Fig. 5C, 5D). Neuronal differentiation of *Ring1B*$^{Δ/Δ}$ stem/progenitor cells, however, was not accompanied by glial differentiation, assessed as GFAP immunoreactive cells (data not shown). Differentiation, in the absence of mitogens, of *Ring1A*$^{-/-}$*Ring1B*$^{Δ/Δ}$ OB stem/progenitor cells, showed a pronounced phenotype with neurons possessing long processes, fewer astrocytes and the absence of oligodendrocytes (supporting information Fig. 6). Together, the results suggest that Ring1B (and Ring1A) contribute to the stability of the undifferentiated state of neural stem/progenitor cells.

Gene Expression Analysis of Ring1B-Deficient OBSCs

Genome-wide mRNA profiling of OB-derived neurospheres under proliferating conditions by microarray analysis showed 972 probes derepressed or repressed more than twofold in *Ring1B*$^{Δ/Δ}$ cultures compared with control spheres. GO analysis showed an enrichment of categories related to neuronal differentiation and to cell proliferation (Fig. 6A, supporting information Table 1). For instance, Neurod1, a transcription factor specific for neurogenesis [45], Tubb3, the Tuj1 antigen, and Ina (internexin neuronal intermediate filament protein, alpha), well-known markers of neuronal differentiation, were among the genes derepressed in Ring1B-deficient cells. Also, effectors of the Notch signaling pathway, such as Hes5, were repressed in mutant cells, which is consistent with previous observations showing the large impact that their inactivation has on the self-renewal of NSCs [46, 47]. Among cell cycle regulators, Cdkn1a, an inhibitor of cyclin-dependent kinases (CDKs), which regulate progression through the G_1 phase of the cell cycle [48], was the one more clearly derepressed. To validate the microarray analysis data, we carried out QPCR on a number of select targets (Fig. 6B). Among transcriptional regulators with relevance in neural progenitor differentiation, we studied *Neurod1*, *Eomes/Tbr2*, *Id4*, *Prdm16*, *Ascl1/Mash1*, *Zfhx3/Athf1*, and *Nr2f2*, all of which were upregulated in mutant neurosphere cultures, except *Ascl1/Mash1*. Genes encoding neuron-specific filaments, *Tubb3* and *Ina*, were also derepressed. Of the CDK-encoding genes analyzed (data not shown for *Cdkn1c/p57*, *Cdkn2b/p15*, and *Cdkn2c/p18*), only *Cdkn1a/p21* was confirmed to be upregulated. Finally, transcripts for the Notch effectors, *Hes5*, *Hes1*, and *Hey1*, were found to be repressed in an RT-QPCR analysis of Ring1B-deficient neurosphere cultures (Fig. 6B). These data show that, in the absence of Ring1B, neural progenitors upregulate an inhibitor of cell cycle progression, attenuate Notch signaling, and cannot maintain their undifferentiated state, all of which can contribute to the impaired self-renewal and reduced proliferation abilities observed in Ring1B-deficient OB stem/progenitor cells.

Considering that Ring1B is a transcriptional repressor, it appears likely that repressed genes in mutant cells are indirect targets of Ring1B. To distinguish between direct (Ring1B bound) and indirect (not Ring1B bound) targets, we used a

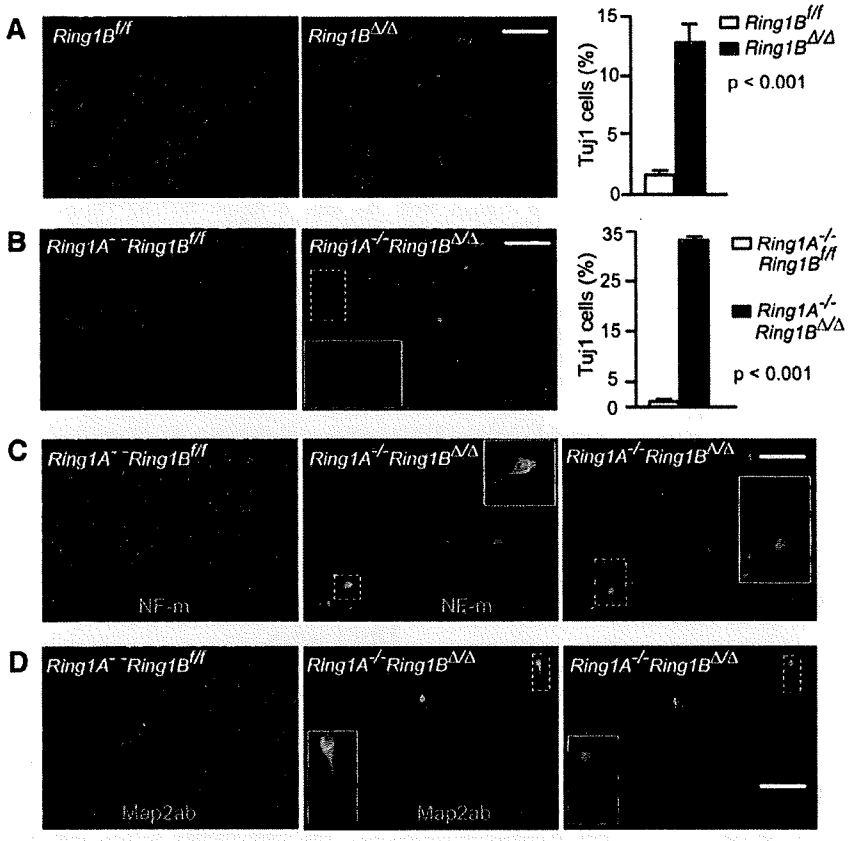

Figure 5. Accelerated neuronal differentiation in Ring1B-deleted olfactory bulb stem cells grown in the presence of mitogens. (**A**): Ring1B-deficient cultures contained a subpopulation of Tuj1^{+} cells ($n = 6$; $p < .001$), suggesting premature differentiation even under proliferative conditions. (**B**): Unscheduled differentiation was enhanced by the inactivation of both Ring1A and Ring1B, leading to the expression of Tuj1 by one third of the cells ($n = 3$; $p < .001$), of which some possessed prominent neurites (inset). (**C**, **D**): Compound *Ring1A* and *Ring1B* mutant cultures stained with neuronal differentiation markers (NF-m and Map2ab). Representative fields showing cells that express both Tuj1 and NF-m (**C**) or Tuj1 and Map2ab (**D**) in the presence of mitogens. Scale bars = 50 microns. Abbreviations: DAPI, 4′,6-diamino-2-phenylindole; Map2ab, microtubule-associated protein 2ab; NF-m, neurofilament medium chain.

chromatin immunoprecipitation (ChIP) on chip approach. Supporting information Figure 7A shows the results on a subset of chosen genes. Whereas the promoter regions of a number of genes derepressed in *Ring1B*$^{\Delta/\Delta}$ cultures were bound by Ring1B (*Neurod1*, *Id4*, *Eomes*, *Prdm16*, *Nr2f2*), other upregulated loci (*Tubb3*, *Ina*, *Athf1*, or *Cdkn1a*) showed very little bound Ring1B, suggesting that their derepression is secondary to *Ring1B* inactivation. Of interest is the fact that despite Ring1B occupancy of promoter regions of *Neurog1* and *Neurog2*, two important regulators of neural development, their expression was found unaltered in Ring1B-deficient cells. On the other hand, no Ring1B was found recruited to the chromatin of genes encoding Notch pathway members, such as *Hes1*, *Hes5*, *Hey1*, and *Dll3* (supporting information Fig. 7A), all of which were repressed in Ring1B-deficient neurospheres.

Analysis of chromatin modifications by ChIP analysis on select targets (supporting information Fig. 7B) revealed increases in the promoter proximal levels of H3K4me3, a histone marker typically associated with transcriptional activation in mutant cells. Levels of H3K27me3, a histone marker usually associated with transcriptional repression, however, showed little variation between mutant and control cultures. On the other hand, *Ring1B* inactivation lead to only a partial reduction in global levels of monoubiquitylated histone H2A (supporting information Fig. 7C), and complete depletion was only observed when both Ring1A and Ring1B were deleted (supporting information Fig. 7C). The data suggest that gene expression changes in directly regulated Ring1B targets are accompanied by chromatin modifications and that Ring1A partially compensates for the absence of Ring1B in mutant neurosphere cultures. Overall, the data suggest that Ring1B contributes to the maintenance of self-renewal and modulation of developmental potential of OBSCs throughout an intricate network of regulatory events that may be under both direct and indirect control by Ring1B.

In Vivo Altered Proliferation/Differentiation of Neural Progenitors in *Ring1B* Mutant Embryos

To assess the impact of Ring1B inactivation in an in vivo setting, we analyzed fetuses 4 days after tamoxifen treatment of gestating females, of which some received a dose of BrdU 4 hours before perfusion. For these experiments, we used *Ring1B*$^{f/f}$ females that were mated to *Ring1B*$^{f/f}$, *Rosa26::CreERT2* males, so that mutant (Cre-expressing) and wild-type (without the Cre-expressing transgene) embryos were obtained in the same litter. Efficient Ring1B inactivation assessed by immunohistochemistry is shown in supporting information Figure 4B. Proliferation was evaluated by staining with an antibody that recognizes the phosphorylated form (at serine 10) of histone H3 (PH3), a mitotic marker. We found a lower number of labeled cells (54.5%; $p < .001$) (Fig. 7A), which agrees with the reduced proliferation seen in neurosphere assays. These PH3^{+} cells expressed nestin (supporting information Fig. 8), indicating their neural stem/progenitor nature. The numbers of PH3^{+} cells were also lower (25% lower than in controls; $p < .05$) in the cortex of *Ring1B*$^{\Delta/\Delta}$ 17.5 dpc fetuses (sections, $n = 16$ from two animals of each genotype). This reduction in mitotically active cells was still more

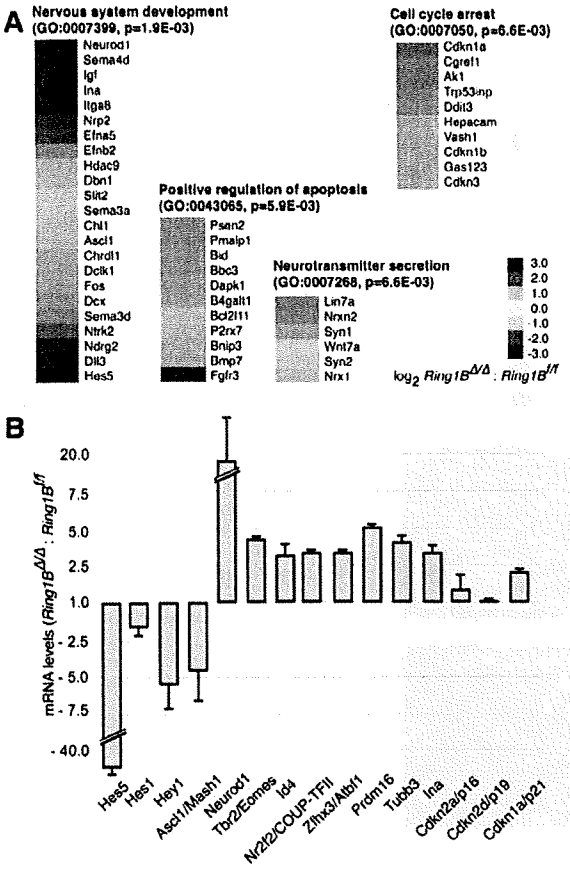

Figure 6. RNA profiling analysis of Ring1B-deleted neurospheres. (**A**): Gene ontology (GO) analysis of genes whose expression changed more than two-fold in neurosphere cultures of olfactory bulb stem cells isolated from 13.5 days postcoitum (dpc) *Ring1B*$^{f/f}$ mouse embryos, 4 days after 4-hydroxy-tamoxifen (4HT) treatment. The four most significantly altered GO categories (biological process) by statistical analysis are shown. (**B**): Validation of Ring1B target genes indicated by analysis of RNA expression profiling, using quantitative polymerase chain reaction. Changes in expression levels are displayed as the ratio between normalized (for β-actin expression) levels of select transcripts in Ring1B-deficient and wild-type neurosphere cultures. Error bars depict the standard error of the mean between three experiments. Expression analysis of the same subset of Ring1B target genes was also carried out with Ring1B-deficient neurospheres grown under differentiating conditions, with 13.5 dpc dissected olfactory bulb tissue and with *Ring1A* and *Ring1B* compound mutant neurospheres grown under proliferating conditions (supporting information Table 2).

pronounced in 17.5 dpc *Ring1A*$^{-/-}$*Ring1B*$^{\Delta/\Delta}$ embryos than in controls (supporting information Fig. 9).

We also analyzed differentiation in *Ring1B*$^{\Delta/\Delta}$ embryos. Gliogenic differentiation was analyzed in 17.5 dpc embryos, at the beginning of astrocyte formation in the developing embryo. The sections, stained with an anti-GFAP antibody, showed a lower number of stained cells in mutant embryos than in wild-type embryos (41% of those in wild-type embryos; $p < .001$) (Fig. 7B). In addition, using an alternative assay that allows the identification of differentiating, unexpanded, progenitors (32), we found a 50% lower ($p < .05$) number of GFAP$^+$ cells in 17.5 dpc mutant OBs, compared with controls ($n = 9$ control cultures and $n = 7$ *Ring1B*$^{\Delta/\Delta}$ cultures). In contrast, neurogenesis, assessed by immunostaining with anti-Tuj1 antibodies, was found to be augmented in mutant OBs, which showed greater numbers of Tuj1$^+$ cells (Fig. 7C, 7D). To test if the increase in TuJ1$^+$ cells and the reduction in GFAP$^+$ cells were due to changes in the proliferation of OB progenitor cells in vivo and/or to an increased tendency of progenitors towards neurons, dividing cells were labeled with BrdU and their differentiation was examined 4 hours later. As seen in Figure 7D and 7E, the number of BrdU$^+$ cells was 50% lower in sections from mutant embryos, whereas the fraction of BrdU$^+$ cells that expressed TuJ1 was significantly greater than that of control embryos, suggesting that neuronally biased differentiation may be responsible for the lower numbers of GFAP$^+$ cells. A similar analysis to identify doubly BrdU$^+$ and GFAP$^+$ cells could not be done because the acid treatment of sections needed to detect BrdU interferes with the weak GFAP immunostaining of sections at this developmental stage. The impaired proliferation of neural progenitors in mutant embryos, the augmented neuronal generation, and the decreased glial differentiation establish Ring1B as a promoter of proliferation of embryonic neural progenitors and as a modulator of their differentiation potential in the developing OB.

Discussion

Self-renewal of stem cells involves the coordination of signaling pathways that ensure cell replication while maintaining their differentiating potential. We report here that inactivation of Polycomb subunit Ring1B impairs proliferation and self-renewal of embryonic OB neural stem/progenitor cells, concurrently with the loss of developmental potential and accelerated neuronal differentiation. Our observations suggest that the self-renewing function of embryonic neural stem/progenitor cells uses Polycomb epigenetic regulation to balance cell cycle control and differentiation commitment.

Self-Renewal and Proliferation

Major differences between the self-renewal dynamics of embryonic/fetal and adult stem cells lie in their programs of proliferation control [4]. Thus, fetal stem cells proliferate actively and expand their populations throughout development, whereas proliferation of adult stem cells is tightly regulated, dividing rarely, as demanded by tissue homeostasis. The Polycomb role in self-renewal of NSCs is mostly known through the analysis of *Bmi1*-mutant adult mice, which show a lower number of neural stem/progenitor cells whose self-renewal ability is also impaired. These defects are thought to result from premature senescence induced by the accumulation of products of the *Ink4a* locus, which is normally repressed by Bmi1 [23–25], that are responsible for decreased neurogenesis during ageing [49].

Our studies on neural embryonic stem/progenitor cells show that their proliferation, both in neurosphere assays and in the OB, depends, at least in part, on Ring1B. Furthermore, self-renewal, as assessed in secondary neurospheres under clonogenic conditions and in two stages of single cells, is impaired in the absence of Ring1B. These results are in line with those resulting from acute inactivation of Bmi1 in embryonic stem/progenitor cells expressing Bmi1 shRNAs [26]. In both cases, loss of function of either *Bmi1* or *Ring1B* (this report) leads to little or no upregulation of the products of the *Ink4a* locus. Instead, Cdkn1a/p21, an inhibitor of the CDKs that determine progression of the cell cycle through the G_1 phase, is upregulated. A difference, however, between Bmi1

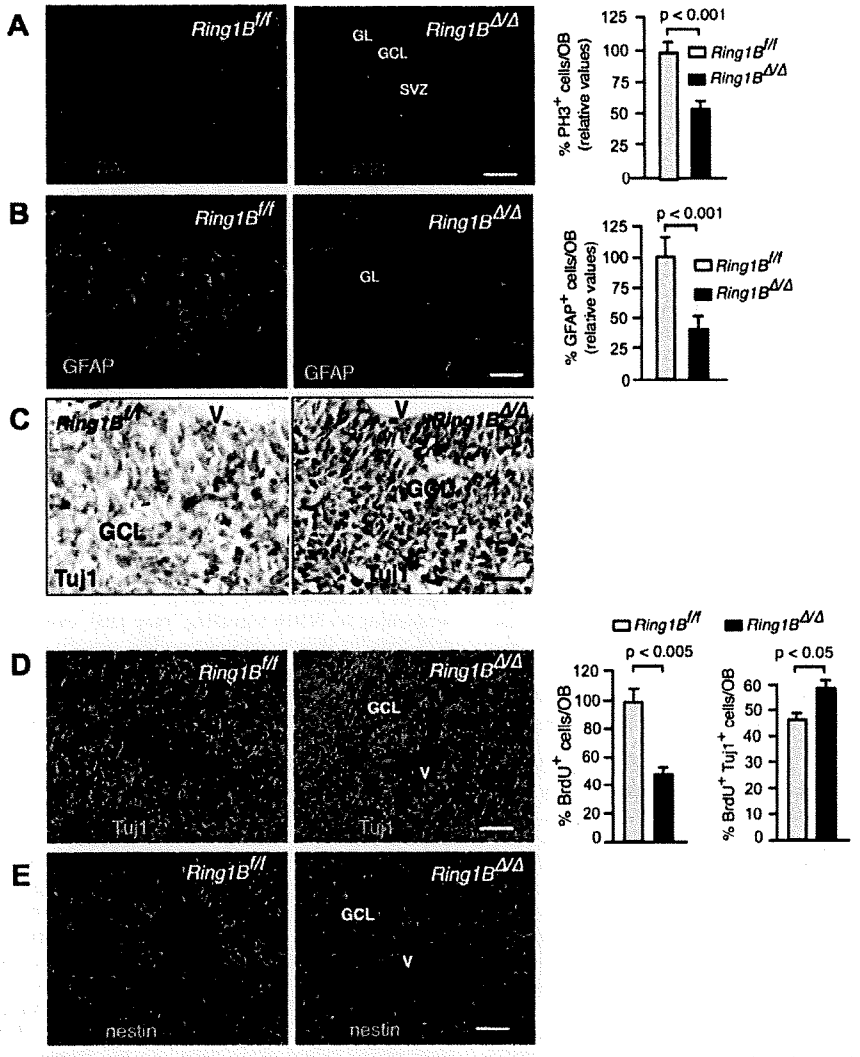

Figure 7. Proliferation and cell differentiation in the fetal OB. **(A):** Decreased cell proliferation of 17.5 dpc OBs from mice injected with tamoxifen, assessed by immunostaining with antibodies against PH3 ($n = 24$ sections from three animals of each genotype; $p < .001$). **(B):** GFAP immunostaining revealed reduced gliogenesis in 17.5 dpc Ring1B-deficient OBs ($n = 24$ sections from three animals of each genotype). **(C):** Histochemical analysis of 17.5 dpc OB, showing a higher number of Tuj1-expressing cells in the subventricular and granular cell layers of mutant OBs. **(D):** Confocal microscope images of 17.5 dpc OB sections from mice injected with BrdU 4 hours before sacrifice to identify proliferating cells (assessed by anti-BrdU immunostaining) and newly differentiating cells (immunostained with Tuj1 antibodies) from dividing progenitors ($n = 20$ sections from two mutant and two control animals). Histograms show that, in *Ring1B*$^{\Delta/\Delta}$ OBs, a significant fraction of proliferating cells had begun to differentiate into neurons (right) despite the generalized decrease in cell proliferation in the mutant OB (left). **(E):** Confocal microscope images of neural progenitors (nestin-expressing cells) in 17.5 dpc OBs from mice injected with BrdU 4 hours before sacrifice, showing the lower proliferative rate in mutant OBs. Scale bars = 100 microns **(A)**, 20 microns **(B)**, 25 microns (C), and 38 microns **(D, E)**. Abbreviations: BrdU, 5′-bromo-2-deoxyuridine; DAPI, 4′,6-diamino-2-phenylindole; dpc, days postcoitum; GCL, granule cell layer; GFAP, glial fibrillary acidic protein; GL, glomerular layer; OB, olfactory bulb; PH3, phosphohistone H3; SVZ, subventricular zone.

and Ring1B activities promoting fetal NSC self-renewal appears to be suppressing apoptotic programs, which seems to depend more on Bmi1 [26] than on Ring1B, given the indistinguishable apoptotic rates of wild-type *Ring1B* mutant progenitors. In this regard, it seems peculiar that a set of deregulated genes in Ring1B-deficient OB-derived neurospheres belongs in the GO term of positive regulation of apoptosis. On the other hand, negative regulation of Cdkn1a/p21 by Polycomb products may occur through indirect mechanisms because, at least for Ring1B, we found no evidence of association with gene promoter regions. Cell cycle control of adult neural stem/progenitor cells is controlled, at least in part, by CDKIs encoded by *Ink4a* and *Cdkn1a/p21* [24, 50, 51]. However, our data, together with previous observations such as the growing impact of Bmi1 inactivation on self-renewal of developing neural progenitors while

Cdkn1a/p21 upregulation decreases over time [26] and the lack of *p16Ink4a* upregulation in the fetal brain from *Bmi1*$^{-/-}$ mice [24] and fetal *Ring1B*$^{\Delta/\Delta}$ OB-derived neurospheres (Fig. 7B), suggest that negative regulation of *Cdkn1a/p21* is a prevalent mechanism during expansion of embryonic neural stem/progenitor cells.

Maintenance of Differentiation Potential

Our striking observation that Ring1B-deficient embryonic neurospheres growing under proliferative conditions express differentiation markers (β-tubulin III) suggests defective maintenance of the undifferentiated state central to stem/progenitor cells. Unscheduled differentiation in the absence of Ring1B was, however, only partial, because when its paralog, Ring1A, was also inactivated, signs of differentiation affected a larger fraction of cells in the culture, some of which expressed morphological features of neurons and expressed not only β-tubulin III but also neuronal markers characteristic of differentiated neurons, such as Map2ab and neurofilament. Nevertheless, Ring1B-deficient neurospheres derepress a number of transcription factors relevant to the differentiation of neural progenitors and the specification of neuronal fates, in particular, *Neurod1*, which appear as Ring1B direct targets. Acute inactivation of *Bmi1*, in contrast, does not lead to similar differentiative defects, although downregulation of progenitor markers such as Nestin and Neurog2 were observed [26]. It is worth noting that the fewer GFAP$^+$ cells and the lack of O4$^+$ cells together with the presence of large process-bearing Tuj1$^+$ cells in Ring1A- and Ring1B-deficient cells growing without mitogens suggest that neuronal differentiation is much favored in these mutant progenitors. Most likely this relates to the observation that the neural cell fate appears to be the default specification during neural differentiation [52, 53]. The accelerated neuronal differentiation seen here in Ring1A- and Ring1B-deficient neural progenitors parallels the differentiative defects seen in Ring1B-deficient ES cells [44, 54], except for the fact that the failure to prevent differentiation leads toward a defined, rather than a more disordered, cell fate, possibly due to restrictions on the developmental potential of tissue-specific stem cells.

A possible explanation for the premature differentiation of Ring1B-deficient neural progenitors is that some of the signaling pathways involved in stem cell self-renewal are affected. Of these, the Notch pathway appears to be a good candidate, considering the accelerated differentiation of NSCs defective in one or more components of the Notch signaling pathway [46, 55]. Active Notch signaling downregulates proneural gene expression, thus inhibiting neuronal differentiation (reviewed in [56–59]). Indeed, expression analysis of Ring1B-deficient neurosphere cultures, under proliferating conditions, shows that stationary mRNA levels of Notch effectors, such as Hes5, are downregulated. Considering that Ring1B is a transcriptional repressor, it is likely that downregulation of Notch effectors occurs through indirect effects, perhaps through the upregulation of uncharacterized transcriptional repressors or microRNAs. In this regard, it is worth noting that regulation of Notch target genes is preferentially modulated by postranslational modifications in subunits of transcriptional complexes, leading to the dismissal/recruiting of coactivators and corepressors [60]. Although Bmi1 and Ring1B associate with each other for efficient H2A monoubiquitylation [18, 22, 27, 61], the fact that Bmi1 inactivation does not have a similar impact on Notch signaling may be due to functional substitution by Bmi1 paralogs known to act as cofactors in H2A modification [61, 62]. Alternatively, it is possible that Ring1B complexes other than PRC1 are involved, at least in part, in transcriptional control of the regulatory network associated with the program defined by Notch signaling.

Coordinated regulation of cell cycle exit and differentiation of progenitors is essential for the generation of appropriate numbers of cells. Thus, in epithelial cells, Notch1 has been found to activate p21 expression [63]. In contrast, in our *Ring1B*$^{\Delta/\Delta}$ neural stem/progenitor cells, Notch signaling downregulation occurs with p21 upregulation. However, rather than an inconsistency, both observations may only be a reflection of the known context dependency of Notch signaling activity, by which it can serve both as an oncogene and also as a tumor suppressor [64]. In neural stem/progenitor cells, it is not known whether slowing proliferation, perhaps due to upregulation of inhibitors of cell proliferation (Cdkn1a/p21), and unscheduled differentiation are related processes or whether they are independent of each other. It has been noted that cell cycle lengthening of neural progenitors may contribute to a switch from proliferative to neuron-generating cell division [65]. If this is the case, it is conceivable that downregulation of the Notch pathway may occur as a consequence of a primary alteration in the cell cycle. This is illustrated by *Hes1* repression mediated by p107 [66], an inhibitor of G_1–S transition. Alternatively, premature neurogenesis, induced by weakening of Notch signaling, may lead, even in the presence mitogens, to slower, neurogenic-like cell divisions previous to eventual cell cycle withdrawal.

Our results show that, in the absence of mitogens, loss of function of *Ring1B* has little effect on cell differentiation under nonclonal conditions (as a fraction of neural and glial derivatives and the total number of differentiated cells). An exception is the significantly lower number of oligodendrocytes formed in *Ring1B*$^{\Delta/\Delta}$ than in control neurosphere cultures, a phenotype strongly enhanced in *Ring1A*$^{-/-}$*Ring1B*$^{\Delta/\Delta}$ mutant cultures. This observation could not be confirmed in vivo, because olidogendrocyte formation peaks postnatally and the administration of tamoxifen to gestating mice leads to defective delivery of pups (also, tamoxifen treatment at very early stages leads to a severe developmental defect in our *Ring1B* mutant mouse line). However, a similar phenotype was recently reported for neural progenitors depleted of Ezh2 (the Polycomb protein with activity of histone H3K27 methyltransferase), which were found to be unable to differentiate into oligodendrocytes [67]. In vivo, we found alterations in astrocyte and neuron differentiation in the OB. First, fewer GFAP$^+$ cells were detected in 17.5 dpc mutant fetuses that were exposed to tamoxifen at day 13.5 of development, compared with controls, suggesting defective astrocytic differentiation. In contrast, neurogenesis at the same developmental stage, assessed as Tuj1$^+$ cells, appeared enhanced. Although *Ring1B*$^{\Delta/\Delta}$ OB progenitor proliferation is lower than in controls, they contain more double Tuj1$^+$BrdU$^+$ cells, suggesting that the tendency toward neuronal differentiation of mutant progenitors may account for the lower number of GFAP$^+$ cells in mutant OBs. Finally, alterations in the differentiating ability of *Ring1B*$^{\Delta/\Delta}$ progenitors were also observed in the lower developmental potential of clonally derived mutant neurospheres.

In summary, we have shown that the Polycomb protein Ring1B promotes proliferation and self-renewal of embryonic neural stem/progenitor cells through the repression of cell cycle inhibitors and maintenance of signaling pathways (Notch) that prevent differentiation. The data also suggest that Ring1B is part of the mechanisms that regulate competence of embryonic neural stem/progenitor cells to generate neurons and glia over developmental time.